Evaluating seasonal sea-ice cover over the Southern Ocean ~~from~~ at the Last Glacial Maximum

Ryan A. Green[1,2,3], Laurie Menviel[1,4], Katrin J. Meissner[1,2], Xavier Crosta[5], Deepak Chandan[6], Gerrit Lohmann[7,8], W. Richard Peltier[6], Xiaoxu Shi[7], and Jiang Zhu[9]

[1]Climate Change Research Centre, University of New South Wales, Sydney, Australia
[2]ARC Centre of Excellence for Climate System Science, Sydney, Australia
[3]Earth and Planetary Sciences, University of California, Santa Cruz, USA
[4]The Australian Centre for Excellence in Antarctic Science, University of Tasmania, Hobart, Tasmania 7001, Australia
[5]Université de Bordeaux EPOC, UMR 5805, Pessac, France
[6]Department of Physics, University of Toronto, 60 St. George Street, Toronto, Ontario, M5S 1A7, Canada
[7]Alfred Wegener Institute, Helmholtz-Zentrum für Polar- und Meeresforschung, Bremerhaven, Germany
[8]Institute for Environmental Physics, University of Bremen, Bremen, Germany
[9]Climate and Global Dynamics Laboratory, National Center for Atmospheric Research, Boulder, Colorado, USA

Correspondence: Ryan A. Green (rygreen@ucsc.edu)

Abstract. ~~Sea-ice cover over the Southern Ocean responds to and impacts Southern Ocean dynamics and , thus, mid to high latitude climate in the Southern Hemisphere. In addition, sea-ice cover can significantly modulate the~~ Southern hemispheric sea-ice impacts ocean circulation and the carbon exchange between the atmosphere and the ocean. Sea-ice is therefore one of the key processes in past and future climate change and variability. As climate models are the only tool available to project future climate ~~changes~~change, it is important to assess their performance ~~in simulating past changes~~against observations for a range of different climate states. The Last Glacial Maximum (LGM, ~21,000 years ago) represents an interesting target as it is a relatively well documented period with climatic conditions ~~and a carbon cycle~~ very different from pre-industrial conditions. Here, we ~~study the changes in seasonal Antarctic~~ analyse the LGM seasonal Southern Ocean sea-ice cover as simulated in numerical ~~PMIP3 and LOVECLIM simulations of the LGM, and their relationship with windstress and ocean temperature~~ simulations part of the Paleoclimate Modelling Intercomparison (PMIP) phases 3 and 4. We compare the model outputs to a recently updated compilation of LGM seasonal Southern Ocean sea-ice cover and summer sea surface temperature (SST) to assess the most likely LGM Southern Ocean state. Simulations and paleo-proxy records suggest a fairly ~~well constrained~~ well-constrained glacial winter sea-ice edge ~~at 51.5~~between 50.5° ~~S (1 sigma range: 50~~and 51° ~~-55.5° S). Simulated~~ S. However, the spread in simulated glacial summer sea-ice ~~cover however differs widely between models~~is wide, ranging from almost ~~no sea ice~~ ice-free conditions to a sea-ice edge reaching ~~55.5~~53°S. ~~The austral summer multi-model mean~~ Combining model outputs and proxy data, we estimate a likely LGM summer sea-ice edge ~~lies at ~60.5~~between 61° ~~S (1 sigma range: 57.5~~and 62° ~~-70.5° S). Given the lack of strong constraints on the~~ S and a mean summer sea-ice extent of 14-15 x 10^6 km^2, which is ~20-30% larger than previous estimates. These estimates point to a higher seasonality of southern hemispheric sea-ice during the LGM than today. We also analyse the main processes defining the summer sea-ice edge ~~based on~~ within each of the models. We find that summer sea-ice ~~proxy records, we extend our model-data comparison to summer sea-surface temperature. Our~~

analysis suggests that the multi-model mean summer sea ice provides a reasonable, albeit upper end, estimate of the austral summer cover is mainly defined by thermodynamic effects in some models, while the sea-ice edge allowing us to conclude that the multi-model mean of austral summer and winter sea-ice cover seem to provide good estimates of LGM conditions. Using these best estimatesis defined by the position of Southern Ocean upwelling in others. For models included in both PMIP3 and PMIP4, this thermodynamic or dynamic control on sea ice is consistent across both experiments. Finally, we find that there was a larger the impact of changes in large-scale ocean circulation on summer sea ice within a single model is smaller than the natural range of summer sea-ice seasonality during the LGM compared to the present daycover across the models considered here. This indicates that care must be taken when using a single model to reconstruct past climate regimes.

1 Introduction

Antarctic sea ice plays an important role in the Earth's climate system, affecting marine productivity, air-sea gas exchange, ocean circulation, heat transport, surface albedo, carbon uptake and deep-water formation. Specifically, it air-sea heat fluxes, surface water density, and surface albedo. It can both impact and respond to changes in Southern Ocean bottom-water formation and Southern Ocean (SO) circulation, and it has been shown to impact the concentration of atmospheric CO_2 on glacial-interglacial timescales (e.g., Ferrari et al., 2014).

therewith impact large-scale heat transport and ocean carbon uptake. While Arctic sea-ice cover has significantly decreased over the last few decades, Antarctic sea-ice cover has been more dynamic. Antarctic sea-ice cover It slowly expanded from the late 1970's until 2014, before sharply decreasing (Parkinson, 2019; Cavalieri and Parkinson, 2012; Wang et al., 2019). This decline in 2016, and then sharply declined for the next three years (Eayrs et al., 2021). Doddridge and Marshall (2017) have shown that, on a seasonal timescale, SO sea-ice cover is thought to be due to an intense was responding to changes in the southern annual mode (SAM)negative phase as changes in Ekman transport lead to higher sea-surface , with a positive phase of the SAM leading to lower SO sea surface temperatures (SST) around Antarctica (Doddridge and Marshall, 2017). and a larger sea-ice extent. However, on longer timescales, a positive phase of the SAM can lead to a SO warming due to the enhanced upwelling of relatively warm circumpolar deep waters (Ferreira et al., 2015). Due to continued anthropogenic emissions of carbon dioxide, the southern hemispheric westerly winds are projected to strengthen and to shift towards positive phases of the SAM (Zheng et al., 2013), impacting Southern Ocean SO circulation and sea-ice cover further (Mayewski et al., 2017). Given that the Southern Ocean SO has accounted for 43% ± 3% of ~40% of the oceanic anthropogenic CO_2 uptake between 1870 and 1995 (Sabine et al., 2004; Frölicher et al., 2015; Mikaloff-Fletcher et al., 2006; Landschützer et al., 2015) (Landschützer et al., 2015; Sabine et al., 2004; Frölicher et al., 2015; Mikaloff-Fletcher et al., 2006; Sabine et al., 2004; Watson et al., 202 , it is crucial to better understand the processes that impact Antarctic sea-ice cover. Understanding past Specifically, seasonal changes in sea ice can significantly affect SO dynamics through buoyancy (Marzocchi and Jansen, 2017) and lead to changes in the atmosphere-ocean carbon exchange (Haumann et al., 2016). Understanding changes in sea ice and their natural drivers , at different timescales and under different boundary conditions , will therefore will allow us to better project future sea ice changes.

The Last Glacial Maximum (LGM, ~~19~~21,000 ~~to 23,000~~ years ago) featured large continental ice-sheets over North America and Eurasia (e.g., Carlson and Winsor, 2012; Clark et al., 2009), as well as an extended Antarctic ice-sheet (Bentley et al., 2014), and an atmospheric CO_2 concentration of ~185 ppm (Marcott et al., 2014). Despite significant progress in characterizing the LGM sea-surface conditions (e.g., Waelbroeck et al., 2009), oceanic circulation ~~(e.g., Howe et al., 2016; Lynch-Stieglitz et al., 2007; Menvi~~ (e.g., Howe et al., 2016; Lynch-Stieglitz et al., 2007; Meissner et al., 2003; Menviel et al., 2017; Skinner et al., 2017), and mechanisms leading to a lower atmospheric CO_2 concentration (e.g., Kohfeld and Chase, 2017), significant uncertainties remain.

~~For the first time in 1981,~~ Some of these uncertainties lie in characterizing seasonal Antarctic sea ice~~at the LGM was reconstructed using proxy data (CLIMAP-Project-Members, 1981). Since then, there has been significant progress and the most recent reconstruction mainly uses diatom assemblages and statistical methods to reconstruct summer and winter~~ . While LGM Antarctic sea ice was first reconstructed in 1981 (CLIMAP-Project-Members, 1981), the proxy compilation of Gersonde et al. (2005) is nowadays routinely used to provide estimates of LGM sea-ice ~~extent during the LGM (Gersonde et al., 2005; Benz et al., 2016)~~ ~~. Reconstructions suggest a significantly extended Antarctic sea-ice~~ cover~~in austral winter, reaching as far north as ~48-49° S in the Atlantic and Indian sectors of the Southern Ocean (Gersonde et al., 2005; Allen et al., 2011; Ferry et al., 2015; Nair et al., 2019; Xiao et , but only a limited amount of~~ . Since 2005, additional SO sea-ice ~~cover for austral summer (Gersonde et al., 2005; Benz et al., 2016)~~ ~~. However, there is an obvious lack of adequate records implying that summer~~ data has been published (Allen et al., 2011; Benz et al., 2016; , and recently merged into an updated compilation (Lhardy et al., 2021). Within this updated sea-ice compilation, certain cores also contain summer SST estimates. We use this sea-ice proxy data along with the summer SST proxy data to better constrain the minimum and maximum LGM sea-ice cover~~is poorly constrained~~.

~~Though~~ Although paleo-proxy records are an invaluable tool to reconstruct the climate system, they are sometimes scarce or completely absent over entire regions. Climate models can help fill these gaps, as they provide a full 3-dimensional and dynamically consistent representation of the climate system. ~~The~~ However, as climate models are not perfect representations of reality, it is important that we continually evaluate their performance. Additionally, the Paleoclimate Intercomparison Project (PMIP) has been set up to evaluate and compare model performances across consistent boundary conditions (Kageyama et al., 2017). Results from the PMIP phase 4 are currently being released (Kageyama et al., 2020), while phases 1-3 are ~~currently~~ available to the public (https://pmip3.lsce.ipsl.fr).

PMIP2 LGM simulations suggested that simulated LGM Antarctic sea-ice cover did not reflect the zonal variability nor the seasonality seen in proxy reconstructions (Roche et al., 2012). PMIP3 LGM simulations have also been analyzed, however not regionally, with results highlighting large inter-model differences in annual-mean, minimum and maximum Antarctic sea-ice area~~and the impact of these differences on ocean stratification and circulation (Marzocchi and Jansen, 2017).~~

~~No study has yet looked in detail into the seasonal changes in Antarctic~~ , and suggesting most PMIP3 models underestimate austral winter sea-ice cover ~~as~~ in comparison to proxy data (Sime et al., 2016; Marzocchi and Jansen, 2017). Therefore, a regional analysis of seasonal LGM sea ice simulated by PMIP3 models is lacking. Furthermore, no seasonal sea-ice analysis of PMIP4 simulations under LGM boundary conditions ~~.~~ has been performed yet.

Here, we ~~provide an overview of austral summer and austral winter conditions, corresponding to~~ assess the minimum and maximum ~~LGM Antarctic~~ SO sea-ice ~~cover as simulated by~~ extent as simulated in LGM PMIP3 ~~models and an additional~~

~~Earth system model (LOVECLIM). We~~ and PMIP4 experiments. To better assess intra- versus inter-model variability, a suite of LGM sensitivity experiments performed with the LOVECLIM model of intermediate complexity are also included. The PMIP3, PMIP4 and LOVECLIM experiments are compared to available sea-ice and SST paleo-proxy data, allowing us to determine the best model-data fit. Combining models and proxy data, we can provide an updated estimate of seasonal SO sea-ice cover during the LGM. Furthermore, we analyze the processes that lead to ~~these differences, focusing on the simulated~~ the inter-model differences in summer sea-ice ~~cover during austral summer and compare the results to the latest available paleo-proxy data~~extent at the LGM.

2 ~~Materials and~~ Methods

2.1 LGM numerical simulations~~and proxy data~~

In this study, we include all PMIP3 and PMIP4 LGM simulations which provide sea-ice variables in the PMIP3 and PMIP4 database (Table 1). Each LGM simulation follows ~~the~~ either PMIP3 ~~protocol (https://wiki. lsce.ipsl.fr/pmip3/doku.php/pmip3:design:21k:fi~~ ~~with the models being forced with orbital parameters set to values corresponding to 21, 000 years ago, concentrations of atmospheric greenhouse gases of 185 ppm for CO_2, 350 ppb for CH_4, and 200 ppb for N_2O with LGM Northern Hemispheric ice-sheet geometry and albedo (Abe-Ouchi et al., 2015).~~

or PMIP4 protocol (Kageyama et al., 2017; Braconnot and Kageyama, 2015). The PMIP3 protocol calls for all models to use the same ice sheet reconstruction, while the PMIP4 protocol allows for the use of either the original PMIP3 ice sheet to facilitate comparison with earlier simulations, or one of the newer reconstructions ICE-6G_C (Argus et al., 2014; Peltier et al., 2015) and GLAC-1D (Ivanovic et al., 2016). In total, data from eight models ~~were obtained (11 different simulations,~~ was obtained for PMIP3 and from six models for PMIP4 (Table 1). ~~When~~ Three models submitted two different simulations ~~were available for the same model~~ to PMIP3 (CCSM4, GISS-E2-R, MPI-ESM-P). These simulations differed because of a difference in the initial state (CCSM4), or small changes in the physics of the model (GISS-E2-R and MPI-ESM-P)~~, data was averaged to yield~~ . Following Sime et al. (2016), we chose to average the simulations for the models who submitted two LGM runs, yielding one output per model~~in order to prevent overweighting any single model.~~ .

We also include ~~two additional LGM numerical~~ three additional LGM simulations performed with ~~an~~ the Earth system model of intermediate complexity, LOVECLIM (Goosse et al., 2010). ~~Similar to the PMIP3 models, these simulations were forced with appropriate LGM orbital parameters, Northern Hemispheric ice-sheet topography and albedo, and greenhouse gases (Menviel et al., 2017).~~ LOVECLIM consists of an ocean general circulation model, a dynamic-thermodynamic sea-ice model, coupled to a quasi-geostrophic atmospheric model, ~~and~~ a dynamic vegetation model ~~(Goosse et al., 2010). These simulations were performed to study the impact of changes in oceanic circulation on the carbon cycle,~~ and a carbon cycle model (Goosse et al., 2010). One of the LOVECLIM simulations follows the PMIP4 protocol, while two additional simulations were obtained by transiently forcing the model between 35 and ~~thus also allow us to estimate the impact of changes in oceanic circulation on Southern Ocean properties. Two simulations are used: i) one with a weaker~~ 20 thousand of years before present with appropriate boundary conditions (i.e. orbital parameters, Northern Hemispheric ice-sheet topography and albedo)

Table 1. Models and experiments used analysed in this study. The last column indicates , the name of PMIP phase they pertain to, and the simulation(s)ice-sheet forcing that was used. AO: coupled Atmosphere-Ocean GCMs (vegetation is prescribed)When applicable, AOV: coupled Atmosphere-Ocean-Vegetation GCMs the ensemble member (vegetation rip-PMIP3/ripf-PMIP4) for the model is computed by specified. IcIES is the Ice sheet model)for Integrated Earth system Studies forced by climatic outputs from MIROC (Abe-Ouchi et al., 2013) . QAOV: quasi geostrophic The atmospheric model coupled to ocean GCM with dynamic vegetation modelCO_2 concentration (pCO_2) for PMIP3 and PMIP4 experiments is 185 ppm and 190 ppm, respectively. pCO_2 for the two LOVECLIM sensitivity experiments is given.

Model Name	Modelling Center Reference	Type Ice sheets	Grid Reference(sPMIP phase and rip(f)	Ensembles Additional comments
CNRM CNRM-CM5	Centre National de la Recherche Météorologique (CNRM) & Centre Européen de Recherche et de Formation Avancée en Calcul Scientifique (CERFACS), France Voldoire et al. 2013	AO PMIP3	Atm: 256x128xL31 Ocean: 362x292xL42 (Voldoire et al., 2013) PMIP3 r1i1p1	
GISS-E2-R	Goddard Institute for Space Studies (GISS), USA Schmidt et al. 2014, 2011; Ullman et al. 2014	AO PMIP3	Atm: 144x90xL40 Ocean: 288x180xL32 PMIP3 r1i1p150/r1i1p151	(Schmidt et al., 2014, 2011) r1i1p150 - PMIP3-ice sheet / r1i1p151 - ICE-5G ice extent with lower Laurentide Ice Sheet altitude
IPSL-CM5A-LR	Institut Pierre Simon Laplace (IPSL), France Dufresne et al. 2013; Kageyama et al. 2013	AOV PMIP3	Atm: 96x96xL39 Ocean: 182x149xL31 (Dufresne et al., 2013; Kageyama et al., 2013) PMIP3 r1i1p1	
MIROC-ESM-P	Japan Agency for Marine-Earth Science and Technology, Atmosphere and Ocean Research Institute (The University of Tokyo), and National Institute for Environmental Studies	AOV PMIP3	Atm: 128x64xL80 Ocean: 256x192xL44 (Sueyoshi et al., 2013; Watanabe et al., 2011) PMIP3 r1i1p1	

(Menviel et al., 2017). During the 35 ka spinup the atmospheric CO_2 concentration was set at 190 ppm, after which CO_2 was a prognostic variable. In these simulations the oceanic circulation was altered by i) adding 0.05 Sv of freshwater to the North Atlantic to simulate a weaker and shallower North Atlantic Deep Water (NADW) formation at the LGM ~~than~~ compared to pre-industrial ~~, obtained by adding 0.05 Sv of freshwater to the North Atlantic~~ (simulation V3LNAw in Menviel et al. 2017, here referred to as ~~LOVECLIM1~~weakNA), ii) ~~one with weaker LGM NADW and Antarctic Bottom Water (AABW) formation, obtained~~ by adding 0.05 Sv of freshwater to the North Atlantic, 0.1 Sv to the ~~Southern Ocean~~SO, as well as by weakening the southern hemispheric westerlies by 20% ~~(~~to simulate a weaker LGM NADW and Antarctic Bottom Water (AABW) formation (simulation V3LNAwSOwSHWw in Menviel et al. 2017, here referred to as ~~LOVECLIM2).~~ weakNA_AB). Atmospheric CO_2 was calculated prognostically in these experiments and equals 203 ppm in weakNA and 191 ppm in weakNA_AB, compared to 185 ppm in the PMIP3 protocol, and 190 ppm in the PMIP4 protocol. These two simulations will be referred to as the "LOVECLIM sensitivity runs". They were chosen because they provided the best model-data fit against a range of paleo-proxy records, including phosphate, $\delta^{13}C$, radiocarbon ventilation ages, and eps(Nd) (Menviel et al., 2017, 2020), thus indicating an appropriate oceanic circulation representation. The three LOVECLIM simulations can provide information on the impact of oceanic circulation differences, and thus inter-model differences, on SO sea-ice and SST versus intra-model differences.

To ease the comparison, we ~~interpolated~~ used bilinear interpolation to standardize each model to a 1° x 1° grid with the ~~software CDO~~ CDO software (Climate Data Operators, Schulzweida et al. 2014).

2.2 Proxy data

The numerical simulations are compared to a compilation of 149 proxy records covering the LGM (See Table S1 in the Supplement, ~~Allen et al. 2011; Benz et al. 2016; Ferry et al. 2015; Xiao et al. 2016; Gersonde et al. 2005; Ghadi et al. 2020; Nair et al. 2019). Of these, quantitative sea-surface temperature was reconstructed in~~ Allen et al. 2011; Benz et al. 2016; Ferry et al. 2015; Gersonde et al. 2). Quantitative SST was reconstructed at 138 locations, ~~proxy~~ proxies for winter sea-ice presence or concentration ~~was available in~~ were available at 149 locations and ~~proxy~~ proxies for summer sea-ice presence ~~was available in~~ were available at 132 locations. ~~Sea-surface temperatures~~ SSTs were derived from diatom-based transfer functions (Crosta et al., 1998; Esper and Gersonde, 2014a) while winter and summer sea-ice extent were derived either from the relative abundance of sea-ice indicator diatoms, respectively the *Fragilariopsis curta* group and *F. obliquecostata* (Gersonde et al., 2005), or diatom-based transfer functions whenever possible (Crosta et al., 1998; Esper et al., 2014b). Relative abundances of the indicator diatoms ~~greater than~~ above 3% are thought to indicate the ~~common~~ presence of sea ice ~~(average~~ over the core site (mean sea-ice extent north of the core site) while relative abundances between ~~2~~ 1 and 3% suggest the episodic presence of sea ice ~~(~~over the core site (mean sea-ice edge south of the core site but maximum sea-ice ~~extent~~edge north of the core site). In this study, we characterize the relative abundance of >3% as evidence of ~~paleo~~ sea ice and the relative abundance between ~~2~~ 1 and 3% as evidence for possible ~~paleo~~ sea ice. Quantitative values were considered to indicate the presence of winter sea ice when they were above the root mean square error of prediction (RMSEP) on the validation models, generally around 10% for winter sea ice (Crosta et al., 1998; Esper et al., 2014b). Quantitative values were always below the RMSEP of ∼10% for summer sea ice ~~on~~ in the

Table 2. Austral winter and austral summer months used for each model. ~~The contour colour for each model corresponds to Figures 1 and 2.~~

~~Model name~~ PMIP3 models	Austral winter	Austral summer	~~Contour color~~ PMIP4 models	Austral winter
~~CNRM~~ MIROC-ESM-P	September-October	February-March	~~Black GISS-E2-R~~ MIROC-ES2L	September-Octob
IPSL-CM5A-LR	August-September	February-March	~~Green~~ IPSL-CM5A2	August-Septembe
~~MIROC-ESM-P~~ MPI-ESM-P	September-October	February-March	~~Blue~~ MPI-ESM1.2	September-Octob
~~MPI-ESM-P~~ CCSM4	September-October	March-April	UoT-CCSM4	September-Octob
CNRM-CM5	September-October	February-March	~~Dashed pink~~ CESM1.2	August-Septembe
GISS-E2-R	September-October	February-March	AWI-ESM-1	August-Septembe
MRI-CGCM3	September-October	February-March	~~Cyan~~ LOVECLIM	August-Septembe
FGOALS-G2	September-October	March-April	~~Red~~ -	-
~~LOVECLIM1~~ heightweakNA	July-August	~~January-February~~ February-March	~~Dashed cyan~~ -	-
~~LOVECLIM2~~ weakNA_AB	August-September	February-March	~~Dashed green CCSM4~~ -	~~September-Octobe~~

validation model. ~~When calculating the proxy sea-ice extent, a South Pole stereographic projection is used to calculate surfaces. For consistency, a South Pole sterographic projection is also used for the models in Figures 1 and 3.~~

2.3 Definitions of sea-ice edge, extent, seasonality, and regions

We analyze the climatology of Antarctic sea-ice extent, since we do not take polynyas into account, and define the two months of maximum and minimum sea ice for each individual model (Table 2). These two months of maximum and minimum sea ice are used consistently throughout the study and will hereafter be referred to as each model's austral "winter" and "summer", respectively. We note that using a two month average leads to a larger summer and a smaller winter sea-ice extent, compared to what would be obtained from a one month average. However, we believe that a two month average is more appropriate for a comparison with proxy records. We also analyze simulated sea ice within specific regions which we refer to by the ocean basin the region lies in: Atlantic~~Sector, Pacific~~Sector~~,~~, Pacific, and Indian Sector.

The sea-ice edge is defined as the 15% sea-ice concentration isoline. We calculate this by zonally averaging across all longitudes for each latitude band, then determining at which latitude the model simulates a minimum of 15% sea-ice concentration. For model simulations that do not reach 15% of sea-ice concentration in ~~certain~~ some regions of the ~~Southern Ocean~~SO, we average only over the remaining regions with sufficient sea-ice cover~~and classify the resulting latitude as the sea-ice edge for the model~~. For model simulations that do not reach ~~a minimum of~~ 15% sea-ice concentration in any region, we define the latitude of their sea-ice edge as the latitude of the Antarctic coast. It is important to note that although a model's sea-ice edge gives insight into its sea-ice characteristics, it is not always an accurate representation of how much total sea ice a model simulates.

Due to this, we also ~~calculated~~ calculate the total sea-ice extent for each model (using a cut-off limit of 15% in concentration). ~~The proxy~~

To calculate the multi-model mean (MMM), we average sea-ice concentration over each grid cell for all models (PMIP3, PMIP4, and LOVECLIM sensitivity runs separately). We then calculate the 15% sea-ice concentration isoline of each MMM. To calculate the standard deviation, we similarly compute a standard deviation value for each individual grid cell, before adding and subtracting that standard deviation (σ) of sea-ice concentration from the MMM for each grid cell. The +/- 1σ then represents the 15% sea-ice concentration isoline calculated from the MMM +/- 1σ. Notably, this creates a non-symmetric standard deviation isoline as each grid cell has its own MMM (and σ) value, calculated independently from any surrounding grid cells.

3 Results

3.1 ~~Overview of results and comparison to paleo-proxy records~~

Figure 1 shows the austral winter and austral summer mean LGM sea-ice extent as simulated by each ~~of the eight PMIP3 models considered here , the LOVECLIM LGM simulations,~~ model considered here as well as the ~~multi-model mean~~ MMM and one standard deviation for the PMIP3, PMIP4 and LOVECLIM models. For comparison, available paleo-proxy records are overlaid for austral winter and austral summer. The simulated annual mean LGM sea-ice extent is shown ~~in Figure~~ for all the models in Fig. S1.

3.1 Simulated austral winter SO sea-ice extent and comparison with winter sea-ice proxy records

During austral winter, the simulated ~~multi-model mean~~ zonally averaged MMM sea-ice edge for PMIP3 models lies at ~51.5˚S with one standard deviation equating to 1.5˚ north and ~~4~~5˚ south of the ~~multi-model mean (Figure 1b). The standard deviation is not symmetric because it is calculated based on the zonally averaged sea-ice concentration at 15%, which varies with latitude. Outside of the zonally averaged mean, large regional~~ MMM (Figure 1d, Table 3). Regional differences are found ~~. In the GISS-E2-R simulation (dashed black-Figure 1a), very little sea ice is simulated~~ across the models. The standard deviation in the Indian Ocean sector (~~15~~20˚E to ~~75~~147˚E) increases to the south due to GISS-E2-R (cyan) simulating a sea-ice edge reaching 59.5˚S in that sector, compared to the Indian sector MMM of 50.5˚S. The standard deviation south of the ~~multi-model mean also increases to 7˚~~ MMM is also large in the Pacific sector (~~175~~147˚E to ~~140~~68˚W) ~~of the Southern Ocean. This increase in standard deviation south of the multi-model mean is in part due to GISS-E2-R (dashed black-Figure 1a), which simulates a~~ as CNRM-CM5 (black) simulates a sea-ice edge at ~59.5˚S compared to the Pacific sector MMM of ~56.5˚S. There is higher model agreement in the Atlantic sector (68˚W to 20˚E) leading to a standard deviation of only +0.5/-1.5˚ in that region.

Similar to PMIP3 models, PMIP4 models simulate a MMM sea-ice edge at ~~57~~~51˚S ~~within the Indian sector. On the other hand, the simulated~~ during austral winter with a zonally averaged standard deviation of 2˚ north and 5˚ south of the MMM (Figure 1h, Table 2). UoT-CCSM4 (orange) simulates the largest sea-ice ~~edge for all 10 modelsis located further poleward on~~

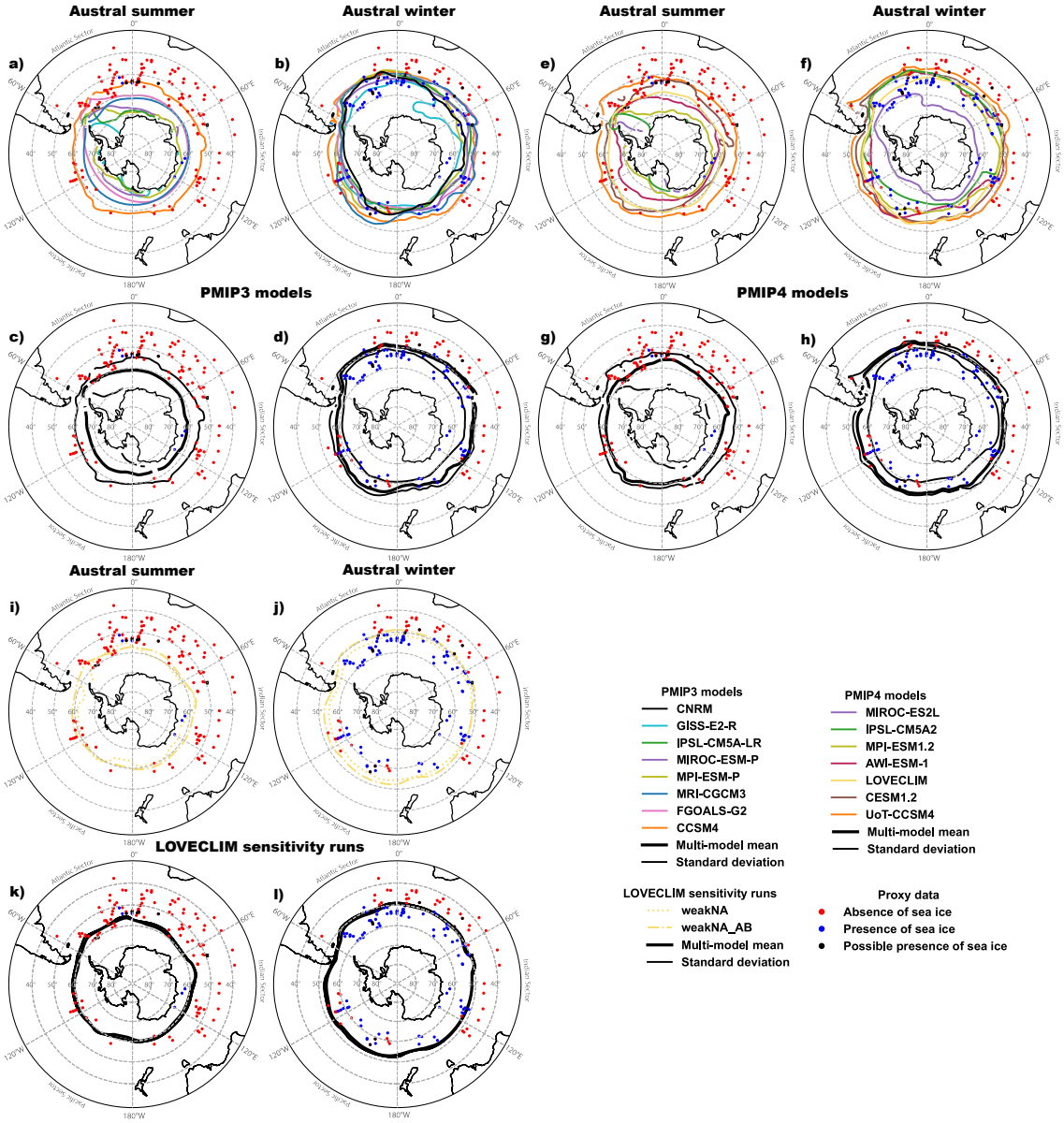

Figure 1. ~~PMIP3~~ Simulated summer and ~~LOVECLIM austral~~ winter sea-ice edge compared to proxy data for PMIP3 (~~a,b~~a-d) ~~,~~ and PMIP4 (e-h) models as well as LOVECLIM sensitivity runs (i-l). The left column for each group shows simulated austral summer sea-ice concentration at 15% (a, c, ~~d~~e, g, i, k) and the right column shows simulated ~~sea ice~~ austral winter simulated sea-ice concentration at 15% (b, d, f, h, j, l). ~~All 10 models are shown in the left panels~~ The top row for each group shows individual model results (a, ~~e~~b,e,f,i,j) ~~and~~ while the ~~multi model~~ bottom row shows the multi-model mean $\pm$ one standard deviation ~~is shown in the right panels~~ (~~b~~c, d, g, h, k, l). Blue, black, and red filled points represent the sediment core proxy data used for the study.

~~the western edge of the Pacific, with the multi-model mean~~ cover with a sea-ice edge at ~48°S. Conversely, MIROC-ES2L (purple) simulates significantly less sea ice than all other models, despite having a slightly extended sea-ice edge north of 60°S in the Atlantic sector. IPSL-CM5A2 (green) also simulates limited sea-ice cover in the Pacific sector. Due to MIROC-ES2L's extended sea-ice edge in the Atlantic and a relatively good agreement between the other six models in that region, the standard deviation is smallest in the Atlantic sector with values of +1°/ -3°.

During austral winter both LOVECLIM sensitivity runs simulate similar sea-ice cover despite the different circulation forcing. The MMM sea-ice edge ~~located at 56~~is simulated at ~51.5°S ~~and the standard deviation decreasing to~~ with a standard deviation of 0.5° north and 1° south~~of the mean in that region~~. PMIP3, PMIP4 and LOVECLIM models thus simulate similar MMM sea-ice edge locations between 51° and 51.5°S. There are slight regional differences due to a few models displaying a different sea-ice edge in a particular sector, however the zonally averaged standard deviations produce similar values for PMIP3 and PMIP4. With only two similar models included in the LOVECLIM sensitivity MMM, the standard deviation is much smaller.

~~In comparison to the proxy data, the austral winter multi-model mean simulates 87% of the sediment core locations correctly. Seven of the ten models show greater than 79%~~ We next compare the simulations with proxy data of sea-ice presence or absence. A relative abundance of *F. obliquecostata* greater than 3% (Figure 1- blue filled circles) indicates the presence of sea ice, relative abundances of *F. obliquecostata* between 1% and 3% suggest the possible presence of sea ice (Figure 1- black filled circles), and core locations with a relative abundance of *F. obliquecostata* < 1% indicate ice-free conditions (Figure 1- red filled circles). We use these data points to calculate a model-data ~~agreement, five of which equal or exceed 80% . At 87% , FGOALS-G2 (red) simulates the highest agreement among individual models and therefore fits the reconstructed~~ sea-ice agreement percentage, based on whether the model simulation correctly or incorrectly simulates the sea-ice ~~extent during austral winter best (~~state at the location of the proxy data. For these calculations, we characterize the possible presence of sea ice (1-3% [*F. obliquecostata*]) as ice-free.

All three MMMs for austral winter display a model-data sea-ice agreement between 83 and 84% (Figure 1, Table 3).

~~All of the models, except GISS-E2-R (dashed black), fall within ± 2° of the multi model mean winter~~ Four proxy data points indicate the presence of sea ice extending past 50°S, all located within the Atlantic sector and into the western-most edge of the Indian sector. Both the PMIP3 and PMIP4 MMMs simulate this feature as their sea-ice edge ~~at 51.5~~extends past 50°S ~~. LOVECLIM1 (dashed cyan) and LOVECLIM2 (dashed green) display a mean simulated winter~~ within the Atlantic sector. In regard to individual model performance, FGOALS-G2 (pink) simulates the highest model-data sea-ice agreement with 87%, corresponding to a simulated sea-ice edge ~~closest to the multi-model mean at 52~~of 50.5°S. With an extended sea-ice edge in the Atlantic and slightly retreated sea-ice edge within the Pacific, FGOALS-G2 seems to most accurately simulate the regional distribution of the proxy data. The data and modelling constraints thus suggest that the LGM austral winter sea-ice (WSI) edge was likely between 50.5°S and 51°S ~~, respectively (Figure 1a and Table 3)~~and the mean LGM austral WSI extent was likely around 35-36 x 10^6 km^2 .

~~A much larger spread between~~

3.2 Simulated austral summer SO sea-ice extent and comparison with summer sea-ice proxy records

A larger spread among the models is obtained during austral summer (Figures ~~1c, 1d)with a multi-model~~ 1a, 1c), with a MMM sea-ice edge at ~~60.5~~~62.5˚S and ~~one~~ a zonally averaged standard deviation of ~~3~~5˚ north and ~~10~~11˚ south of the ~~mean. Similar to the austral winter distribution, the~~ PMIP3 MMM. The largest sea-ice cover is simulated by CCSM4 (~~pink~~orange) with a sea-ice edge at ~55.5˚S. Three models (~~CNRM - black, GISS-E2-R - dashed black,~~ CNRM-CM5, black; GISS-E2-R, cyan; IPSL-CM5A-LR~~–~~, green) only simulate sea ice around the Ross and Weddell Seas and are otherwise ice-free. ~~CNRM~~ CNRM-CM5 (black) simulates the least amount of sea ice at or above 15% concentration with sea ice only simulated in a small region of the Ross Sea (Figure ~~1c). LOVECLIM1 simulates~~ 1a).

The austral summer MMM in PMIP4 models is larger than for PMIP3 with a sea-ice edge at ~59.5˚S ~~, in closest agreement with the multi-model mean~~and a zonally averaged standard deviation of 4.5˚ north and 10.5˚ south of the MMM (Figure 1g, Table 2). Similar to austral winter, UoT-CCSM4 (orange) simulates the largest sea-ice cover with a sea-ice edge reaching ~53˚S while MIROC-ES2L (purple) and IPSL-CM5A (green) simulate the least amount of sea ice with sea ice only found over the Ross and Weddell Sea.

~~For austral summer , only six core locations out of 132 display a relative abundance of *F. obliquecostata* greater than 3% (Figure 1c,d; blue filled circles), indicating the presence of summer sea ice~~ There are slightly larger sea-ice differences between the two LOVECLIM sensitivity runs during austral summer than winter. The MMM sea-ice edge is simulated at ~59˚S with a standard deviation of 0.5˚ north and 1˚ south of the MMM. WeakNA (dotted yellow) has more regional variability than weakNA_AB (dash-dot yellow). Due to the standard deviation being so small for both austral winter and austral summer, the lines are difficult to distinguish from the MMM. The simulated austral summer sea-ice (SSI) ~~. Relative abundances of *F. obliquecostata* are between 2% and 3% in~~ edge is thus more poorly constrained than the winter across the different groups, with a MMM of 59˚ to 62.5˚S, and large standard deviations of 5˚ north and 11˚ south of the mean.

The simulated summer sea-ice extent can also be compared to paleo-proxy records. Only six core locations out of 132 indicate the presence of SSI while seven additional cores from the Atlantic sector of the ~~Southern Ocean (Figure 1c,d; black filled circles), suggesting~~ SO suggest the possible presence of ~~summer sea ice~~SSI. The remaining 119 core locations ~~have a relative abundance of *F. obliquecostata* < 2%~~ indicate ice-free conditions (including 64 cores with 0% ~~), indicating ice-free conditions~~relative abundance of *F. obliquecostata*). Of the six locations indicating the presence of sea ice~~(blue filled circles)~~, three cores are located in the Indian sector at ~63˚S south of the ~~multi-model mean~~MMM for all three model groups, whereas the other three are located in the Atlantic sector at ~53˚S, north of the ~~multi-model mean and the~~ MMM for all three model groups (Figure 1). However, two of the three cores within the Atlantic Sector indicating LGM SSI fall inside the PMIP4 +1 standard deviation ~~(Figure 1d~~contour line (Figure 1g). Five of the seven locations ~~showing~~ indicating the possible presence of SSI ~~(black filled circles) are also~~ are located north of ~~the multi-model mean and the northward~~ all three MMMs, but again on or inside the PMIP4 +1 standard deviation (Figure ~~1d~~1g). We note that the eight locations from the Atlantic sector representing a presence or possible presence of ~~sea ice~~ SSI are bordered by cores suggesting ice-free conditions, possibly indicating a sea-ice tongue protruding from the Weddell Sea. ~~91% of the 119 locations representing ice-free conditions fall north of the multi-model~~

~~mean, leading us to suggest that the multi-model mean at 60.5° S is an upper~~ The reader should bear in mind that with limited proxy data points indicating SSI and multiple models simulating limited SSI, it is not uncommon to record the same summer model-data sea-ice agreement percentage across different model simulations.

With only six proxy data points indicating SSI, the PMIP3 MMM, which displays the smallest SSI extent across MMMs, shows the highest model-data sea-ice agreement (Table 3). In terms of individual models, it is clear some models simulate too much sea ice (CCSM4 and UoT-CCSM4, orange), while other models simulate too little (CNRM-CM5, black; GISS-E2-R, cyan; MIROC-ESM-P and MIROC-ES2L, purple; IPSL-CM5A-LR and IPSL-CM5A2, green). With only six proxy core locations indicating SSI, it is not possible to extrapolate an estimate of the ~~plausible LGM austral summer~~ LGM sea-ice ~~extent. Equatorward of~~ edge strictly based on this data. However, we note that the highest individual model agreement is achieved by MRI-CGCM3 (blue), with an agreement of 98% and a sea-ice edge at 62.5°S, which also corresponds to the PMIP3 MMM. On the other hand, the ~~multi-model mean,~~ data-model agreement significantly drops for models simulating a large sea-ice cover. CCSM4 (~~pink) simulates sea ice~~ orange) and UoT-CCSM4 (orange), with sea ice edges of 55.5°S and 53°S respectively, simulate sea ice in locations where the proxy records suggest ice-free conditions in all sectors of the ~~Southern Ocean,~~ SO. They are thus most likely over-estimating austral ~~summer sea-ice cover. Furthermore, LOVECLIM2 (dashed green), and LOVECLIM1 (dashed cyan) might overestimate the sea-ice cover in the Pacific and Atlantic sectors of the Southern Ocean, while FGOALS-G2 (red)simulates sea ice north of the Weddell Sea where three proxy locations suggest ice-free conditions.~~ SSI cover.

~~In the next section, we focus our analysis on austral summer~~

3.3 Simulated LGM summer SO SST and comparison with proxy records

To better constrain the LGM SSI extent, we look into the proxy estimates of LGM summer SST data. We first assess the relationship between zonally averaged simulated austral summer SSTs in the SO (50°S and 75°S) and the simulated sea-ice ~~extent, evaluating differences between the models and the potential reasons for the observed inter-model spread. We focus our analysis on the thermodynamic and dynamic controls on~~ edge and extent (Figure 2a, b). The relationship between simulated summer SO SST and SSI edge or extent can be approximated by a linear fit, with R^2 values of 0.90 and 0.81, respectively (Figure 2a, b). Similarly, this relationship is also seen during austral winter with R^2 values of 0.80 and 0.88 for the relationship between SST and sea-ice ~~extent, as ocean temperatures exert a significant control on sea-ice formation and melt, and wind-stress affects sea-ice transport.~~ edge and extent, respectively (Figure 5).

3.4 ~~Thermodynamic control on summer sea-ice extent~~

~~It is expected that there should be a robust relationship between~~ The mean LGM summer SO SST can be estimated from proxy records to be 1.52°C ± 0.67°C. Using the mean SST reconstructed from the proxy records and the linear relationship estimated based on the simulations, we calculate a proxy SSI extent estimate of 15.90 10^6 km^2 +/- ~3.25 x 10^6 km^2 and a mean sea-ice ~~cover and SST in the Southern Ocean. We thus first look at the relationship between zonally averaged austral summer SSTs in the Southern Ocean and~~ edge estimate of 61°S +/- ~2.25°. The models closest to these proxy sea-ice ~~edge and extent (Figure~~

~~2a, b).~~ estimates are weakNA (15.73 x 10^6 km^2 yellow plus sign, Figure 2b), FGOALS-G2 (61.5˚S-pink triangle, Figure 2a) and AWI-ESM-1 (62˚S-dark pink square, Figure 2a). LOVECLIM (yellow square) and weakNA_AB (yellow X mark) also fall within the uncertainty of these estimates (Figure 2a, b).

We also look into the meridional profiles of zonally averaged summer SSTs for all models (Figure 2c, d). This is compared to zonally averaged SSTs estimated from proxy data where SST proxy data is available (grey in Figure 2c, d). The SST proxy record suggests a mean SST of 1.44˚C south of 52˚S, with an increase of 1.1˚C per degree of latitude north of 52˚S. The SST latitudinal variations in the models and proxies display significant differences, and none of the models included in this study are able to reproduce the proxy distribution across all latitudes. Among the models, the distribution of zonally averaged SSTs is not consistent over the SO. For example, at 75˚S both PMIP3 and PMIP4 models simulate a SST spread of SST around ~3˚C while at 65˚S both model groups simulate a SST spread of ~6˚C (Figure 2c, d). Between 52˚ and 65˚S, AWI-ESM-1 simulates a mean SST of 1.14˚C, closest to the proxy mean south of 52˚S. Some models are consistently warmer than the proxies (CNRM-CM5, black; GISS-E2-R, cyan; MIROC-ES2L, purple; IPSL-CM5A2, green), whereas others, with a large SSI cover, are colder than the proxy-based SSTs between 55˚S and 60˚S (CCSM4 and UoT-CCSM4, orange; CESM1.2, brown). Furthermore, most models are warmer than the proxies between 55˚S and 45˚S.

~~For seven out of ten simulations, the zonally averaged summer SST between 50˚ S and 75˚ S are between 1.5˚ and 3˚C. By comparison, the mean summer SST estimate from proxy records present in the compilation and falling within this latitudinal band is 1.52 ˚C ± 0.67 ˚C. Two models averages are significantly warmer (GISS=3.71 ˚C and CNRM=5.58 ˚C), and one is significantly colder (CCSM4= -0.52 ˚C). The lower the mean SST, the larger the sea-ice extent with a quasi linear relationship between the two, particularly if excluding the three outliers. Using a linear fit line, and taking into account all the simulations, the summer sea-ice edge and extent are correlated with SST calculated by R^2 values of 0.81 and 0.82, respectively (Figure 2a, b).~~

~~All of the models simulate a mean~~ To look more closely into the regional distribution of SSTs, we plot each model's SO SST overlaid with the available SST data (Figure 3). Due to biological limitations, diatom transfer functions are mostly available in regions with low sea-ice ~~edge near the~~ cover. As such, our proxy summer SST compilation only contains two locations with SST temperatures below 0˚~~C isoline, apart from GISS-E2-R (and CNRM, which simulates a sea-ice edge at the Antarctic coast, Figure 2c). Equatorward of the sea-ice edge, all models display a significant SST increase with decreasing latitudes. Summer SSTs as estimated from proxy records are shown as grey circles (Figure 2c). They suggest a mean SST of 1.41˚C south of 52˚ S, and northward of which they increase significantly with decreasing latitudes. The SST latitudinal variations in the models and proxies display significant differences, with some models being consistently warmer than the proxies (CNRM, GISS-E2-R), whereas others with a significant summer sea-ice cover underestimate the proxy-based SSTs south of 60˚ S (e. g. CCSM4, LOVECLIM, FGOALS-G2).~~

~~Both CNRM and GISS-E2-R seem to consistently over-estimate austral summer SSTs (Fig. 2c). CNRM simulates a mean SST of 5.6 ˚C south of 50˚ S, which explains the minimal amount of sea ice simulated (Fig. 2a, black filled triangle). GISS-E2-R has the second lowest sea-ice extent and simulates a mean SST of 3.7 ˚C~~south of 50. With limited proxy SST data near the freezing point, we instead assess the model-data fit at the 1˚ ~~S (black filled circle). As highlighted in the methods, the sea-ice~~

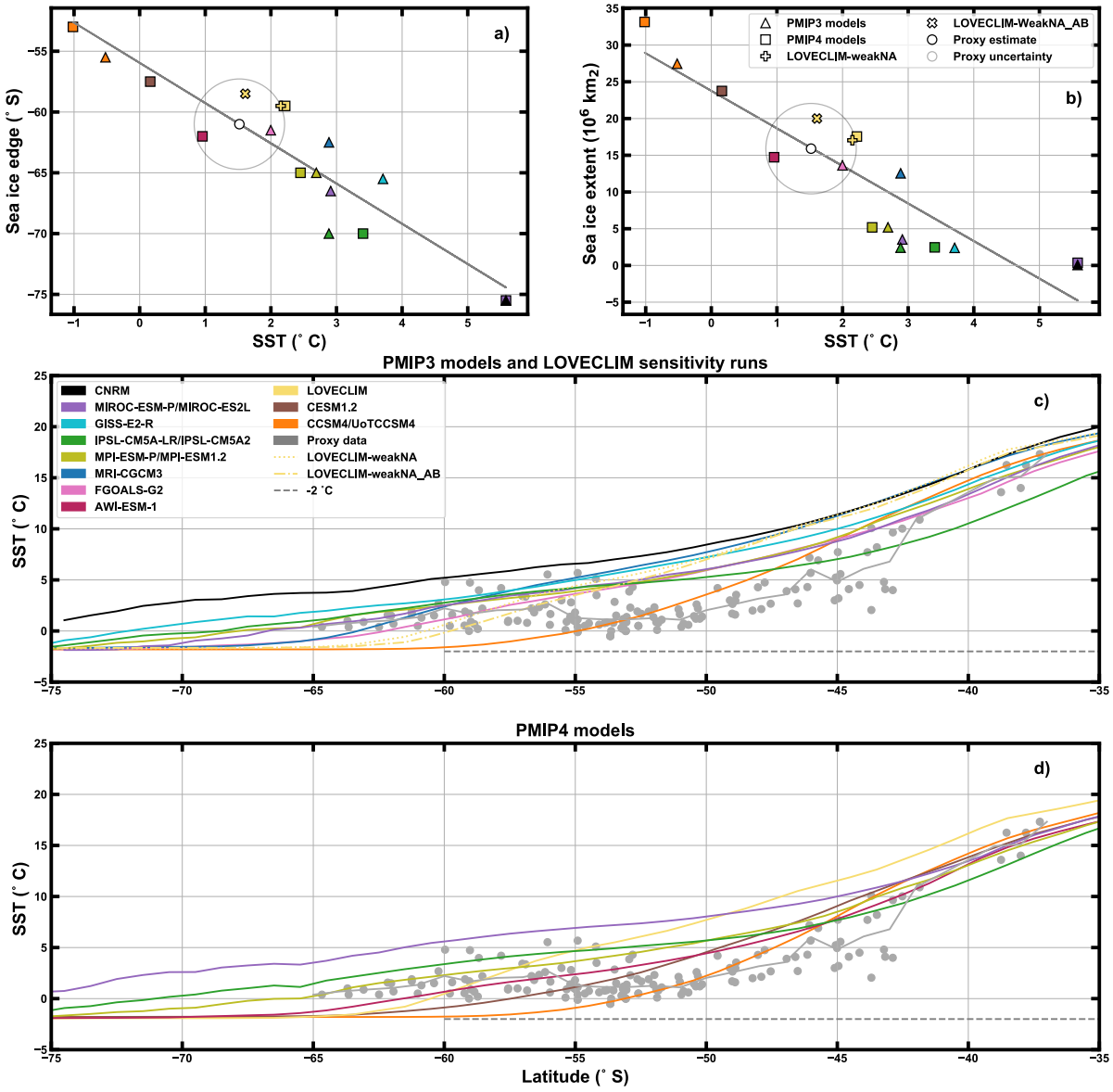

Figure 2. Austral summer sea ice and SST. a) Sea-ice edge vs. SST (50˚-75˚S) b) Sea-ice extent vs. SST (50˚-75˚S). Proxy summer sea-ice extent was estimated using ~~available austral summer sea ice~~ the mean proxy SST value and the linear regression line. Uncertainty from the proxy SST ~~reconstructions~~value is shown in the grey circle. c) and d) Zonally averaged SST values from 35˚-75˚S. ~~Filled triangles represent sea-ice edge for each model.~~ Grey circles represent sediment core proxy data with a grey line fit for the data points.

Table 3. Simulated ~~sea ice~~ seasonal sea-ice characteristics ~~, summer sea surface temperatures~~ and ~~meridional transports ordered~~ austral summer SST, organized based on total sea-ice extent (lowest to highest). Model data agreement is calculated as a percent of the correctly simulated ~~sediment cores~~ sea-ice state at the location of proxies (presence of sea ice or ice-free conditions~~). Statistics on summer sea ice agreement have to be interpreted~~ , with ~~caution as only 6 out~~ possible presence of ~~133 cores suggest sea-ice cover. This implies that models with no simulated austral summer~~ sea ice ~~might have very good agreement with proxy data but could still significantly under-estimate the sea-ice cover~~considered ice-free). The austral summer Southern Ocean SST is ~~latitudinally~~ meridionally averaged over 75˚S to 50˚S. The austral summer sea-ice edge is taken at the mean 15% concentration. Calculated root-mean-squared error (RMSE) values use the summer SSTs from proxy data in comparison to the modeled summer SST output.~~Simulated austral summer zonally averaged meridional advective volume transport is calculated over 75˚ S to 50˚ S for the first 100 m depth for each model. Positive numbers represent equatorward transport and negative numbers represent poleward transport. LOVECLIM results are calculated from annual mean data.~~

~~Model name~~	~~Austral winter~~ Winter sea-ice ~~agreement (%~~edge (˚S)	~~Austral summer~~ Winter sea-ice extent (10^6 km^2)	Winter sea-ice agreement (%)	~~Austral summer average southern ocean SST (˚C) Root mean square value (RMSE) Summer average meridional advective volume transport (Sv) Austral winter~~ Summer sea-ice edge (˚S)	~~Austral summer~~ Summer sea-ice ~~edge (˚ S) Austral summer sea-ice extent~~ extent (10^6 km^2)	Summer sea-ice agreement (%)	Summer SO avg. SST (˚C)	Root mean square error
~~CNRM~~	**PMIP3 models**							
CNRM-CM5	~~67.79~~ 53.5	~~95.45~~ 23.01	~~5.58~~ 65.77	~~3.47~~ 75.5	~~0.5209~~ 0.06	~~53.5˚ S~~ 95.45	~~75.5˚ S~~ 5.58	~~.06047~~ 4.03
GISS-E2-R	~~61.7458.0~~	~~95.4523.61~~	~~3.7157.72~~	~~1.9565.5*~~	~~0.7307~~2.29	~~58˚ S~~95.45	~~65.5˚ S*~~	~~2.391~~

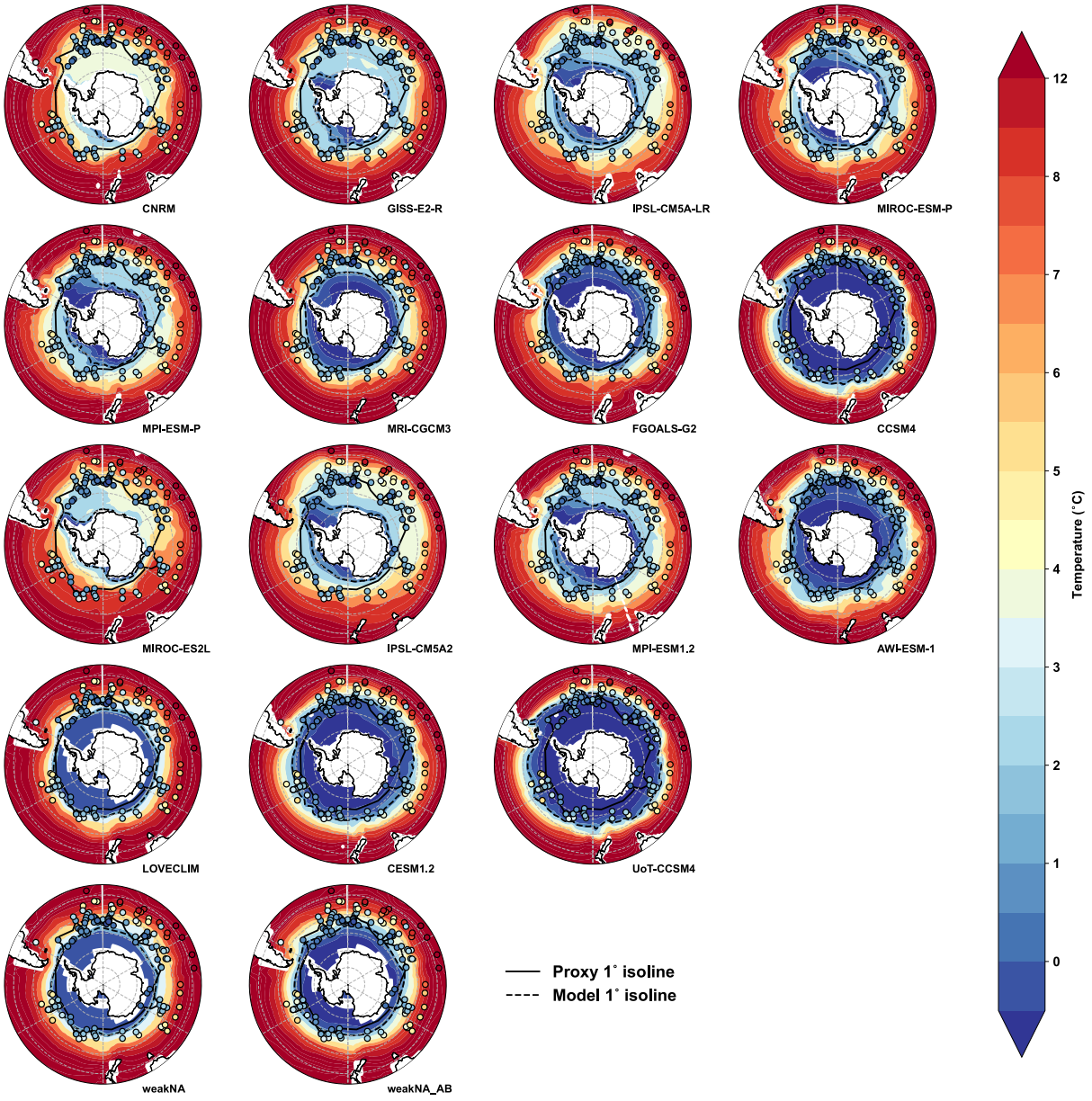

Figure 3. PMIP3, PMIP4 and LOVECLIM austral summer simulated SST with SST reconstruction data overlain. Fill color inside each SST reconstruction data point represents paleo SSTs at each location. Each model's 1˚C isoline is shown with a dotted black contour line and the proxy SST data 1˚C isoline is shown with a solid black contour line.

~~edge is not an all-encompassing metric for sea-ice cover due to our definition. For GISS-E2-R, the sea-ice edge of 65.5~~isoline.

340 We therefore compute the 1˚~~S is calculated only using the Ross Sea, due to the lack of simulated sea ice around the rest of Antarctica in austral summer (Table~~ C isoline based on the proxies (dotted black contour line in Fig. 3~~).~~

~~Conversely, CCSM4 simulates the largest sea-ice cover, reaching 55.5° S, and is the only model displaying a mean SST south of 50° S that is negative (Fig. 2a and 2b, Table 3). The CCSM4 simulated Southern Ocean summer SSTs are significantly lower than the other models south of 48° S and lower than all of the proxy estimates south of 55° S (Figure 2, pink line).~~

~~The IPSL-CM5A-LR model (Figure 2c, green line) simulates a higher zonally averaged SST between the Antarctic coast and 60° S than all of the models, outside of the two warm outliers (CNRM-black and GISS-E2-R-dashed black). These high simulated SST values could potentially explain the low sea-ice cover in the IPSL-CM5A-LR simulation. However, it is interesting to note that IPSL-CM5A-LR displays the lowest SST meridional temperature gradient south of 40° S, thus simulating relatively low SSTs north of 55° S.~~

~~The remaining models (FGOALS-G2-red, MIROC-ESM-P-blue, MRI-CGCM3-cyan, MPI-ESM-P-dashed pink, and the two LOVECLIM simulations: LOVECLIM1, dashed cyan, and LOVECLIM2, dashed green) display a mean SST of 1.5°~~ and compare it to ~~3°C south of 50~~each model's 1°S, ~~and a mean austral summer sea-ice edge between 58.5° and 66.5° S.~~

~~Only 6 out of the 149 LGM samples contained in the compilation show the common presence of SSI (Figure 1c-d, blue filled circles) while 7 samples suggest the episodic presence of SSI (Figure 1c-d, black filled circles). Obviously, it is impossible to infer the Antarctic-wide SSI extent based on such a restricted number of control points. However, very low SSTs (~ 0 - 0.5 °C) were concomitantly reconstructed in the 6 samples showing SSI presence (Gersonde et al., 2005) in agreement with modern environments whereby SSI (Schweitzer, 1995) generally lies south of the 0 °C summer surface isotherm (Locarnini et al., 2010) . We therefore made use of this relation and of summer SST reconstructions (e.g., Benz et al., 2016; Gersonde et al., 2005) to complement the SSI estimates and infer the most probable SSI extent at the LGM. After subtracting the LGM surface of Antarctica (17.10x10^6 km^2; (Bentley et al., 2014)) from the estimated SSI total extent, we arrive at an estimate of the net SSI extent of 11.24x10^6 km^2. This proxy-based net SSI extent is closest to the 12.54x10^6 km^2 extent simulated by MRI-CGCM3. However, the simulated SST (50°-75° S) by MRI-CGCM3 is 1.37 °C warmer than the proxy SST reconstruction (Figure 2b, Table~~ C isoline (solid black contour line in Fig. 3).

~~PMIP3 and LOVECLIM austral summer simulated SSTs with SST reconstruction data overlain. Fill color inside each SST reconstruction data point represents paleo SSTs at each location.~~

~~Figure 3 shows each model's simulated SST compared to the available SST proxy data.~~ The proxy data is regionally variable, with lower temperatures (darker blue points) in the Atlantic and Pacific sectors and higher temperatures (lighter blue, yellow, and red points) in the Indian sector. ~~There~~ Additionally, there are more records at lower latitudes in the Atlantic and Indian sectors~~, which can be seen plotted in Figure S2. Consistent with the previous analysis, CNRM and~~ . Figure 3 confirms that certain models are too warm (CNRM-CM5; GISS-E2-R~~simulate higher SSTs than inferred from proxies, while~~ ; MIROC-ESM-P and MIROC-ES2L; IPSL-CM5A-LR and IPSL-CM5A2) and certain models are too cold (CCSM4 ~~simulates lower temperatures than inferred from proxies.~~

~~Using the proxy data as observations~~and UoT-CCSM4; CESM1.2). The models that simulate a 1°C isoline in good agreement with the proxy records are FGOALS-G2, AWI-ESM-1 and all LOVECLIM experiments (weakNA, weakNA_AB, LOVECLIM). To quantitatively establish how well the models simulate the SST proxy record, we calculate the root-mean-squared error (RMSE) between simulated SSTs and observations ~~for each model~~ (Table 3). The model with the lowest RMSE value

(0.651.40), representing the model for which simulated SSTs fit the reconstructions best, is the FGOALS-G2 model. IPSL-CM5A-LR has the second lowest RMSE value (0.83), potentially due to the extremely cold SSTs north of 52° S. The models with the highest RMSE values are MRI-ESM-P (2.89)and CNRM (3.47)AWI-ESM-1 model. FGOALS-G2 also has a low RMSE value with 1.90.

We further explore the vertical thermal structure of Taking into account the spatial pattern of the sea ice proxy record (Figure 1), the models (Figure 4). The CNRM experiment stands out as simulating significantly warmer conditions everywhere in the ocean compared to any other model, with potential temperatures below 0regional variability of the SST proxy record (Figures 2 and 3), and the RMSE scores from the SST proxy records (Table 3), the most likely LGM SSI edge lies at 61-62°C only deeper than 1000m depth. The GISS-E2-R and ISPL-CM5A-LR experiments, which both simulate low austral summer S, with a mean sea-ice cover and similar Atlantic Meridional Overturning Circulations (AMOC) (Muglia and Schmittner, 2015), display very different temperature structures. This is most likely because NADW, which is brought up in southern high-latitude upper waters via Southern Ocean upwelling, is relatively warm in GISS-E2-R and conversely relatively cold in IPSL-CM5A-LR. This difference in northern end member water masses could explain the relatively weak latitudinal potential temperature gradient in the Southern Ocean in IPSL-CM5A-LR, and the relatively warm conditions in GISS-E2-R. The MIROC-ESM-P extent of 14-15 x 10^6 km^2 such as the ones simulated by the AWI-ESM-1 or FGOALS-G2.

With such large SSI discrepancies among the models, we next look at the potential reasons for inter-model spread. To identify drivers of inter-model sea-ice variability we analyze the thermodynamic and dynamic controls on sea-ice extent, as ocean temperatures exert a significant control on sea-ice formation and melt, and MPI-ESM-P experiments also simulate relatively warm NADW, which could contribute to the relatively low austral summer wind-stress affects sea-ice cover. transport.

Zonally averaged austral summer potential temperature profile for PMIP3 and LOVECLIM models in the Atlantic.

3.4 Drivers of inter-model variability

Although these different thermal characteristics impact model The strength and location of the southern hemispheric westerly and polar easterly winds impact SO circulation, sea ice transport and therefore sea-ice cover, apparent variability between models demonstrates that factors outside of SST and potential temperature also determine the different distribution (Purich et al., 2016; Holl . On the other hand, the presence or absence of sea ice also has a direct influence on surface winds (Kidston et al., 2011; Sime et al., 2016) . Here, we focus on the influence of winds on sea ice through the divergence created by the wind stress curl. Within the SO, divergence leads to upwelling of relatively warm circumpolar deep waters and thus heat loss to the atmosphere. This upwelling can therefore also impact SO sea-ice distribution in these models.

3.5 Dynamic control on summer sea-ice extent

Due to its impact on Southern Ocean circulation and sea-ice transport, the strength and location of distribution. While the latitudinal position and magnitude of southern hemispheric westerlies at the LGM is poorly constrained (Kohfeld et al., 2013; Sime et al., 20 , we want to assess the impact of the southern hemispheric westerly and polar easterly winds also impact simulated windstress curl on ocean dynamics in each model. We thus use the simulated windstress outputs to estimate the location and strength

of the SO upwelling, and its potential impact on sea-ice ~~distribution (Purich et al., 2016; Holland and Kwok, 2012). Figure 5a~~ cover.

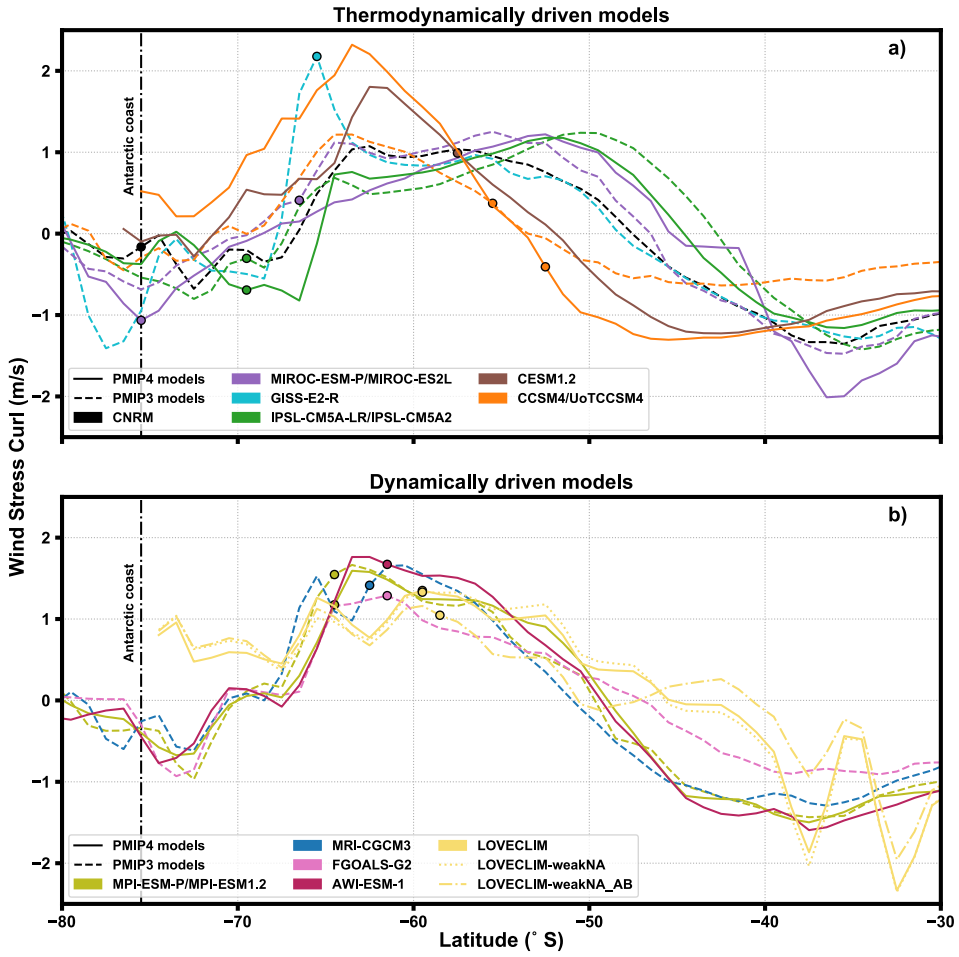

Figure 4. Zonally averaged austral summer wind stress curl vs. latitude for a) models in which mean temperature controls the summer sea-ice edge, b) models in which Southern Ocean upwelling, and associated divergence, impacts the summer sea-ice edge. Each model's sea-ice edge is represented with a filled circle.

Figure 4 shows the zonally averaged austral summer wind stress curl ~~south of 30° S of 6 simulations that display similar mean Southern Ocean SSTs (FGOALS-G2-red, MIROC-ESM-P-blue, MRI-CGCM3-cyan, MPI-ESM-P-dashed pink, LOVECLIM1-dashed cyan, LOVECLIM2-dashed green), with their mean latitude of~~ in the SO with each model's sea-ice edge overlaid. ~~For each of these models, the sea-ice~~ Figure 4b shows LGM experiments in which the SSI edge falls within 2-3 degrees of their zonal mean wind stress curl peak~~(Figure 5a) . The wind stress curl maximum represents divergence of the Ekman transport, indicating the maximum upwelling area. The close link between maximum~~ , indicating that sustained upwelling at 58˚S - 65˚S in these four

models (MPI, FGOALS, AWI, LOVECLIM) most likely impacts summer SST and sea-ice cover. Our analysis suggests that the SSI edge in the MRI-CGCM3 LGM simulation is dynamically driven as its mean SO SST is close to the PMIP3 MMM, and its SSI edge is close to the maximum of the wind stress curl~~and summer sea-ice edge in the FGOALS-G2, MIROC-ESM-P,~~ . However, this result should be taken with caution as in the MRI-CGCM3 ~~, MPI-ESM-P and the two LOVECLIM simulations suggests that Southern Ocean dynamics significantly impact the summer sea-ice edge for these models.~~

~~Zonally averaged austral summer wind stress curl vs. latitude. a) shows the models we expect Southern Ocean dynamics to significantly impact summer sea-ice edge b) shows the models we expect ocean temperatures to play a larger role impacting summer sea-ice edge. Each model's ice edge is represented with a filled triangle.~~

~~In contrast, Figure 5b shows the models we designate as outliers as they are either significantly warmer (CNRM,~~ simulation the coupling between sea ice and wind-stress at the ice/atmosphere interface was absent due to a model bug (Marzocchi and Jansen, 2017) . On the other hand, Fig. 4a shows LGM experiments in which the SSI edge is more than 3 degrees away from the peak of the wind stress curl. The models displayed in Fig. 4a both include LGM experiments with particularly high (CNRM-CM5, black; GISS-E2-R~~) or colder~~ , cyan; MIROC-ESM-P and MIROC-ES2L, purple; IPSL-CM5A-LR and IPSL-CM5A2, green), and low (CCSM4 ~~) than other models and paleo-proxy estimates. IPSL-CM5A-LR is also included here as its~~ and UoT-CCSM4, orange; CESM1.2, brown) SST as identified in section 2. While the sea-ice edge ~~is more than 2° outside of its~~ in GISS-E2-R seems to occur at the maximum of the wind stress curl ~~peak, similar to CNRM and CCSM4 (Figure 5b). GISS-E2-R falls closest to its peak, but with its~~ (cyan dotted line in Fig. 4a), this is an artefact of the averaging. This model's sea-ice edge ~~calculated only from~~ is calculated only based on sea-ice in the Ross Sea ~~, we believe the dynamic effects of the wind stress curl would not have caused the absence of simulated sea ice in the other regions of the Antarctic coast. Apart from the 'pseudo'~~ due to the lack of sea ice elsewhere. Therefore, the true global average sea-ice edge ~~from~~ of GISS-E2-R ~~, this figure shows that the divergence due to the~~ at 15% concentration is at the Antarctic coast, which is more than 3 degrees from its wind stress curl peak. Divergence due to wind stress curl ~~does not~~ thus does not seem to have a large impact on ~~summer sea ice in these modelsas CNRM and GISS-E2-R are likely too warm and~~ SSI extent within the nine experiments (six models) shown in Fig. 4a.

We thus suggest that the location of the SSI edge in experiments displayed in Fig. 4a is thermodynamically controlled, whereas it is dynamically controlled for the ones displayed in Fig. 4b. It is interesting to note that experiments performed by the same models, or different versions of the same models, fall within the same categories: i.e. both PMIP3 and PMIP4 IPSL and MIROC experiments, as well as CCSM4 ~~is too cold. The drivers of sea ice for IPSL-CM5A-LR seem a bit more complex. While IPSL-CM5A-LR simulates the same mean SST south of 50° S as MIROC-ESM-P (2.9 °C, Table 3), IPSL-CM5A-LR~~ and UoTCCSM4 seem to be thermodynamically driven, whereas both PMIP3 and PMIP4 MPI and all LOVECLIM experiments seem to be dynamically driven.

As highlighted in Fig. 2, we find a clear relationship between seasonal sea-ice ~~extent is significantly lower with its edge situated closer to the Antarctic coast compared to MIROC-ESM-P. To understand why these two models simulate different sea-ice dynamics, we calculate the mean meridional advective transport within the upper 100m in the Southern Ocean (~~extent and seasonal SST. Additionally, as surface processes impact temperatures at deeper layers, we also find a statistically significant

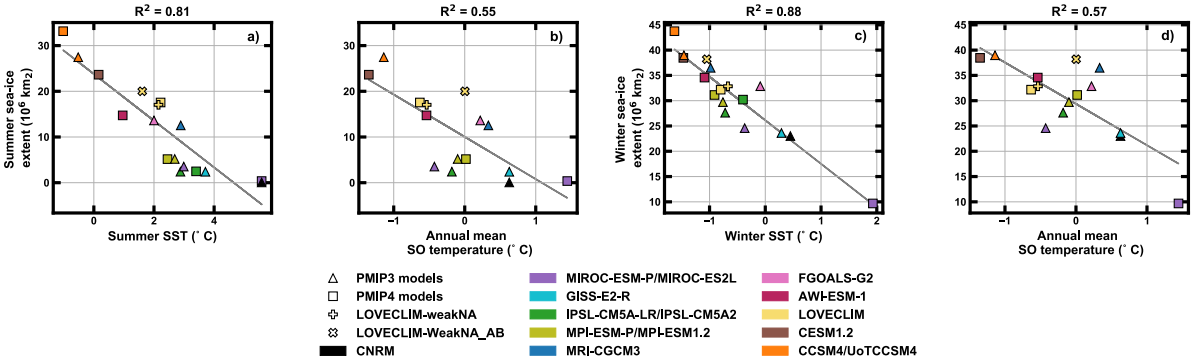

Figure 5. Scatter plot showing the relationship between sea ice, SO SST (averaged over 50-75˚S) and SO temperature (averaged over 50-75˚S and through full water column). Panels a, b show the relationship for austral summer and panels c, d show the relationship for austral winter.

relationship between SO temperature (defined as the ocean temperature zonally averaged between 50˚S ~~to~~ and 75˚S ~~) for each PMIP3 model. We find that all models simulate an equatorward surface transport, apart from IPSL-CM5A-LR, which displays a poleward zonal mean surface transport (Table 3). IPSL-CM5A-LR also displays the most equatorward windstress curl peak, thus potentially explaining the lower than average SSTs north of the windstress curl peak, and higher than average SSTs south of the peak, with advection of lower latitude waterstowards the Antarctic coast.~~

~~We have evaluated the Antarctic seasonal~~ over the whole water column) and both WSI and SSI extent (Figure 5). The larger the sea-ice ~~distributions for eight PMIP3 LGM simulations and two LOVECLIM LGM simulations and compared them with available paleo-proxy records. Apart from one model (~~extent, and thus the lower SO SST, the lower the mean SO temperature. However, SO temperature is partly controlled by AABW temperature and by the latitudinal extent and temperature of circumpolar deep waters. For example, while they display very different sea-ice covers both CCSM4 and GISS-E2-R ~~), which displays little sea ice in the Indian Ocean sector of the Southern Ocean, austral winter simulations are in global agreement with the existing proxy data, with a~~ simulate AABW close to freezing. However, in the GISS-E2-R simulation, the AABW extent is limited and the relatively warm NADW leads to warm circumpolar deep waters (Figure 6).

The interplay between SO surface conditions and seasonal sea-ice ~~edge at ~51.5˚ S (1 sigma range: 50˚–55.5˚ S). FGOALS-G2 (red) best fits the distribution shape of the proxy data across the three regions and is in agreement with 87% of the proxy data points. MRI-CGCM3 (cyan), LOVECLIM2 (dashed cyan),~~ cover modulates AABW temperature. LGM experiments with relatively cold surface conditions and relatively large SSI cover (e.g. CCSM4~~(pink), and IPSL (green) austral winter~~ , LOVECLIM) also simulate cold (< -1˚C) AABW. On the other hand, some LGM experiments with relatively warm conditions still simulate cold AABW due to the large seasonal difference in sea-ice ~~cover also all closely resemble the data distribution and are in agreement with at least 80% of the proxy data points. A previous study found similar results, identifying CCSM4 and MRI-CGCM3 LGM maximum and minimum Southern Hemisphere~~ cover (GISS-E2-R, MIROC-ESM-P). Finally, LGM

experiments with both warm surface SO conditions and low seasonal differences in sea-ice ~~area in closest agreement to the~~
475 ~~paleoreconstructions (Marzocchi and Jansen, 2017)~~cover simulate anomalously warm AABW (CNRM-CM5, MIROC-ES2L).

~~However, the models exhibit large differences in austral summer sea-ice coverage with one model simulating a sea-ice edge at 55~~

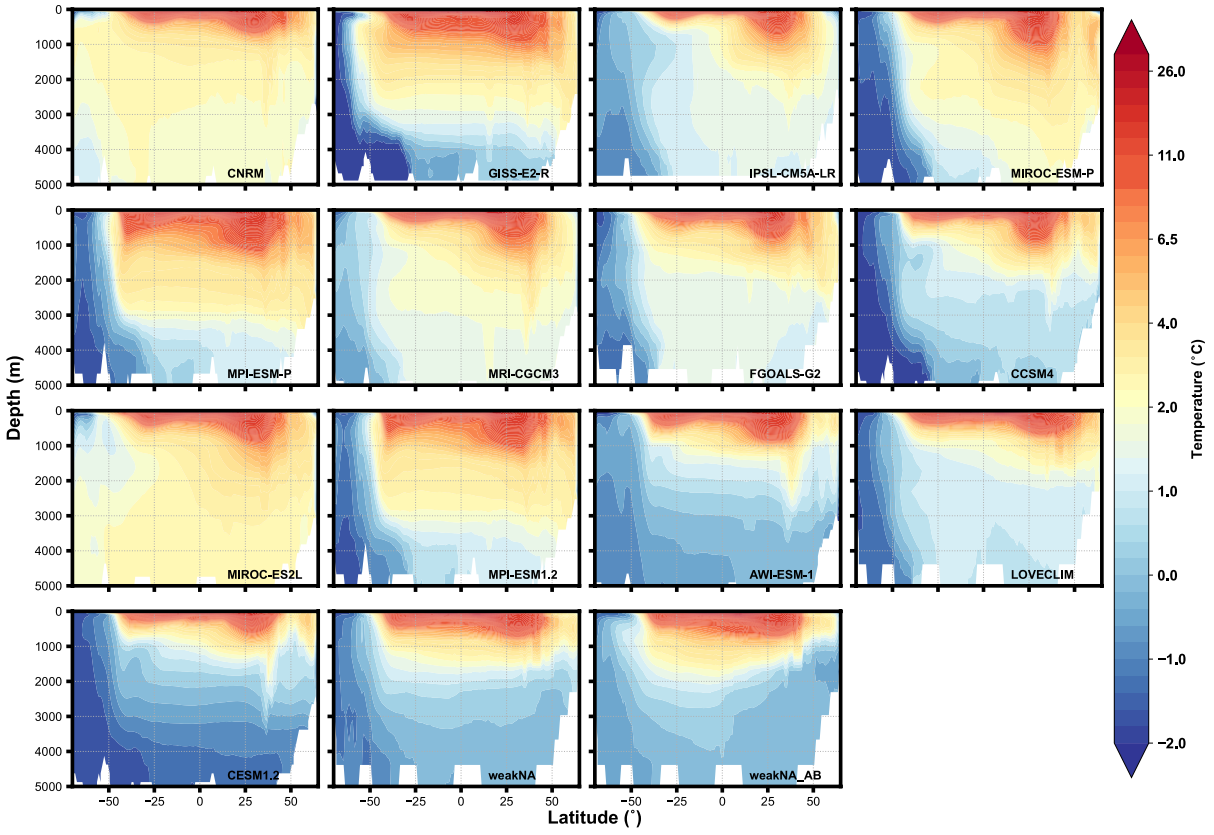

Figure 6. Zonally averaged oceanic potential temperatures (˚C) for PMIP3, PMIP4 and LOVECLIM models in the Atlantic.

4 Discussion and conclusions

We suggest that during the LGM, the likely austral WSI edge was between 50.5˚S ~~(CCSM4), while two others (GISS-E2-R~~
480 ~~and CNRM) simulate an almost ice-free Southern Ocean. Our comparison with available summer~~ and 51.5˚S, with a mean sea-ice ~~records is limited as there are only six sediment core locations that reflect the presence of summer sea ice (Allen et al., 2011; Benz et al., 2016; Ferry et al., 2015; Gersonde et al., 2005; Ghadi et al., 2020; Nair et al., 2019; Xiao et al., 2016). Additionally, these six locations are grouped within two small regions. Three of the cores are located in the Indian sector at ~63~~extent of 35-36 x 10^6 km^2. During austral summer we suggest the sea-edge was likely between 61˚ ~~S, along the Antarctic~~

coastal shelf. The other three are located in the Atlantic sector at and 62°S, with a mean sea-ice extent of 14-15 x 10^6 km^2, similar to the sea ice characteristics simulated by AWI-ESM-1 and FGOALS-G2. This is an improved constraint on LGM SSI extent as we use modeled sea ice in conjunction with paleo-proxy SST and sea ice data to calculate our estimate. Our LGM SSI extent estimate is slightly larger than previous estimates of ~53° S and are bordered by other records suggesting ice-free conditions immediately northward, thus potentially suggesting sporadic 10.2 x 10^6 km^2 (Lhardy et al., 2021) and ~11.1 x 10^6 km^2 (Roche et al., 2012), which only use sea-ice advance to that latitude. In the same way, cores from the Indian and Pacific sectors in which *F. obliquecostata* counts were published suggest ice-free conditions at 60-63° S (Figure 1c,d). Nevertheless, the multi-model mean simulates a summer sea-ice edge at 60.5proxy data to calculate their estimates. Our estimates can also be compared to the average modern austral WSI extent of 18.5 x 10^6 km^2 and the average modern austral SSI extent of 3.1 x 10^6 km^2n (Eayrs et al., 2019).

Our estimate for the LGM SSI edge is a zonally averaged estimate and therefore assumes a fairly circular SSI distribution, similar to that simulated by AWI-ESM-1 and FGOALS-G2 (Figure 1). While the LGM SSI proxy data is limited, Lhardy et al. (2021) suggest the three basins behaved very differently, with a LGM SSI edge at 54°S , which agrees with 92% of the proxy data though it may appear too expanded in the Atlantic, 65-66°S in the Indianand Pacific sectors while not expanded enough in the Atlantic sector of the Southern Ocean. , 63°S in the western Pacific and 66-68°S in the eastern Pacific. If this indeed was the case, our suggested LGM SSI edge would potentially overestimate the sea ice edge in some regions while potentially underestimating it in other regions. Additional proxy data from the Pacific and Indian basins would reduce the uncertainty of our estimate.

To try to better constrain the austral summer Southern Ocean conditions, we compare the simulations with available summer SST reconstructions. This model-data comparison in While the SSI edge is thermodynamically driven for six of the models considered here, it is linked to the position of the maximum windstress curl for the remaining five models (Figure 2 shows that the simulated SST decreases more gradually with latitude than in the proxy reconstructions. However, this figure uses only zonally averaged SSTs. When viewing all of the ocean basins, Figure 3 shows that colder models (LOVECLIM 1 and 2, CCSM4)display a larger simulated SST gradient. As prior research has shown that CMIP5 models display a warm bias over the Southern Ocean (Meijers, 2014), there is potential for this SST gradient discrepancy to diminish as models improve. Our analysis suggests that the models simulating little to no summer sea iceare likely too warm, and thus under-estimate the summer sea-ice edge. The simulated NADW in these models is also quite warm, thus likely leading to a warm bias in the Southern Ocean5). The maximum wind stress curl corresponds to the maximum Ekman transport divergence, leading to deep-water upwelling. This can impact sea ice both thermodynamically and dynamically, as upwelling is often linked with ocean heat release while the Ekman transport divergence can lead to strong equatorward transport of sea ice. Given the uncertainties that surround the magnitude and the position of the Southern Hemisphere westerlies at the LGM (e.g., Kohfeld et al., 2013; Sime et al., 2016), this casts additional uncertainties on the location of the austral SSI edge. Furthermore, paleo records of austral SSI extent used here are mostly restricted to 40°- 60°S, with 95% of the records suggesting ice-free conditions. Due to this, they can only provide an estimate of the maximum SSI extent. Additional proxy records recovered from locations south of 60°S are thus needed to better constrain the SSI extent.

~~The models also~~ Both the PMIP4 and PMIP3 experiments display a relatively large range (~ -2˚ to 4˚C) of temperatures in the deep Atlantic Ocean (Figure ~~4~~6). Only a few paleo-records of deep ocean temperature are available for the LGM, but they suggest ocean temperatures below 0˚C throughout the deep Atlantic ~~(Adkins et al. , 2002). In the Southwest~~ (Adkins et al., 2002). In the southwest Pacific at ODP Site 1123, Mg/Ca records find deep ocean temperatures of -1.1 ± 0.3~~°~~˚C at the LGM (Elderfield et al., 2010). ~~Additional data would help constrain deep ocean temperature and water masses distribution, and thus total ocean heat and carbon content~~The models that simulate warm SO conditions with little sea-ice also simulate a warm bias at depth, even though in some cases a large seasonal (~20 x 10^6 km^2) difference between maximum and minimum sea-ice extent can lead to cooler abyssal temperatures.

~~Our analysis also included two~~ In this study, we also included three LGM experiments performed with ~~LOVECLIM, in which the~~ the Earth system model LOVECLIM. The oceanic circulation was varied ~~by addition of meltwater and changes in~~ in two of these experiments by adding meltwater in the North Atlantic and SO and weakening the southern hemispheric westerly windstress (Menviel et al., 2017). Despite significant differences in oceanic circulation in these ~~two~~ three simulations, with weaker ~~NADW and AABW~~ AABW transport in weakNA_AB compared to weakNA, and weaker Atlantic meridional overturning circulation (AMOC) in weakNA (14.7 Sv) and weakNA_AB (11.2 Sv) compared to the PMIP4 LOVECLIM experiment (26 Sv), the differences in ~~LOVECLIM2 compared to LOVECLIM1, the~~ sea-ice ~~cover differences between these two runs~~ extent between these three experiments are much smaller than ~~compared to other models. Apart from FGOALS-G2, which simulate a very strong LGM AMOC,~~ the ~~LGM AMOC strengths in the other~~ inter-model differences between all PMIP3 ~~models are similar at 21-23 Sv (Muglia and Schmittner, 2015). This indicates that the primary control on LGM austral summer~~ and PMIP4 simulations. This indicates the limitations of performing model-data comparisons with a single model to infer SO climatic conditions.

We further assess the relationship between LGM SSI and AMOC strength (Figure S2, Muglia and Schmittner 2015; Kageyama et al. 202), and find that there is no statistically significant relationship between the two (R^2=0.04). There is however a weak relationship between sea-ice ~~cover is not linked to the strength of the AMOC~~ extent and AMOC depth (Figure S2, R^2=0.17), with a shallower AMOC generally associated with a larger sea-ice extent. A larger sea-ice extent, and thus increased sea-ice formation, could impact the AABW properties and therefore ocean stratification (Marzocchi and Jansen, 2017), as evident from Fig. 5. However, climatic conditions in the North Atlantic are probably the principal driver of AMOC depth (Oka et al., 2012; Muglia and Schmittn . There is also no link between the equilibrium climate sensitivity (ECS) of these models and their austral ~~summer sea-ice~~ SSI cover, with the three models displaying the least amount of sea-ice exhibiting ECS of 3.3˚C for ~~CNRM, 2.1~~CNRM-CM5, 2.7˚C for ~~GISS-E2-R and 4.2~~MIROC-ES2L, and 2.1˚C for ~~IPSL-CM5A-LR~~GISS-E2-R, while the two models with the most sea-ice have an ECS of ~~2.8~~2.9˚C and 3.2 (CCSM4 and ~~LOVECLIM).~~ UoT-CCSM4, respectively, Kageyama et al. 2021).

~~For the models simulating relatively similar austral summer SST values (FGOALS-G2-red, MIROC-ESM-P-blue, MRI-CGCM3-cyan, MPI-ESM-P-cyan, LOVECLIM1-dashed cyan, LOVECLIM2-dashed green), our analysis suggests the location of their respective sea-ice edge is linked to the position of the maximum windstress curl. The maximum wind stress curl corresponds to a maximum Ekman transport divergence, creating maximum upwelling strength in that region. This can impact sea ice both thermodynamically and dynamically, as upwelling is often linked with ocean heat release while the Ekman transport divergence~~

can lead to strong equatorward transport of sea ice into warmer SSTs. Given the uncertainties that surround the magnitude and the position of the Southern Hemisphere westerlies at the LGM (e.g., Kohfeld et al., 2013; Sime et al., 2016), this casts additional uncertainties on the location of the austral summer sea-ice edge.

An integrated view of the model-data comparison suggests that the best fit is obtained for a summer sea-ice edge situated at about 62° S, close to the one simulated by FGOALS-G2, MRI-CGCM3 and Based on our best estimates of LGM WSI and SSI cover over the SO, the multi-model mean. However, as paleo records of austral summer seasonal variation in sea-ice extent are mostly restricted to 40°-60° S, with 95% of the records suggesting ice-free conditions, they can only provide an estimate of the maximum summer sea-ice extent. Additional proxy records recovered from locations south of 60° S are thus needed to better constrain the summer sea-ice extent.

If our reconstruction of LGM summer sea-ice extent is correct, the seasonal variation of the sea-ice edge equals is ~10° latitude, and the and the seasonal variation in sea-ice extent difference equals 20x10is 20-22 x 10^6 km^2. In comparison, the seasonal change in sea-ice extent for present day climate equals ~ 15x1015.4 x10^6 km^2 (Eayrs et al., 2019), thus indicating a larger sea-ice seasonality during the LGM. Such a large sea-ice seasonality would in turn impact Southern Ocean SO dynamics through changes in buoyancy (Marzocchi and Jansen, 2017) as well as the carbon cycle (Haumann et al., 2016). While a large year-round LGM sea-ice cover would contribute to the decreased could contribute to a lower atmospheric CO_2 concentration (Ferrari et al., 2014), the impact of an increased a large sea-ice seasonality on the carbon cycle is not well constrained. The increased seasonality has potential to dampen CO_2 drawdown, depending on the balance between upwelling and subsequent outgassing of carbon rich deep waters and nutrient utilization at the surface (e.g., Menviel et al., 2008). Conversely, the increased seasonality could also amplify carbon drawdown through enhanced brine formation, increasing the density gradient between the surface and deep waters (Galbraith and de Lavergne, 2019), and potentially lowering of atmospheric CO_2 (Bouttes et al., 2012). Despite proxy records showing lower productivity in the Antarctic Zone (Jaccard et al., 2013), increased stratification due to sea-ice melt during spring-summer could enhance nutrient utilization and thus carbon drawdown (Sigman and Boyle, 2000; Abelmann et al., 2015). While some studies have suggested a primary role for LGM sea-ice cover in driving changes in oceanic carbon content (Ferrari et al., 2014), the LOVECLIM experiments presented here have also shown that reduced ventilation of the deep ocean through weaker AABW transport could instead be the primary driver of an increase in deep ocean carbon content (Menviel et al., 2017).

Antarctic sea ice also integrates oceanic and atmospheric processes occurring at high southern latitudes, and as such can also significantly impact Antarctic climate (Bracegirdle et al., 2015). Sea ice has the ability to protect ice-shelves (Massom et al., 2018) and floating ice-shelves play a significant role in buttressing Antarctic outlet glaciers (Scambos et al., 2004). It is thus crucial that models incorporate a good representation of pre-industrial and present-day sea ice, but also manage to correctly simulate past sea-ice extent during both cold periods such as the LGM, and warm periods such as the Last Interglacial (125,000 years ago).

In that regard, it is interesting to note that the models which under-estimate underestimate austral summer Antarctic sea-ice cover at the LGM also under-estimate the austral summer sea-ice underestimate the austral SSI cover under pre-industrial conditions, while the model simulating the largest LGM sea-ice cover also over-estimates overestimates the pre-industrial summer

sea-ice cover (Marzocchi and Jansen, 2017; Goosse et al., 2013)SSI cover (Marzocchi and Jansen, 2017; Goosse et al., 2013; Roche et al., . This implies that targeting a good agreement between model and observations for present day climate should remain a priority.

In this study, we have analysed simulated Southern Ocean winter and summer sea-ice SO WSI and SSI cover in LGM simulations and evaluated the seasonality from LGM numerical simulations and evaluated the output compared the outputs against available proxy reconstruction data. In doing so, we identify thermal and dynamic model characteristics as the potential drivers for inter-model Southern Ocean SO sea-ice differences, in addition to placing further improved constraints on the LGM austral summer and winter sea-ice SSI and WSI extent in the Southern OceanSO. This improved understanding of the relationship between model design and sea-ice dynamics can provide valuable information about the Earth system and important insight into the strengths and weaknesses of models currently used.

Data availability. The ocean and sea ice data for the LOVECLIM sensitivity runs can be found at https://doi.org/10.26190/K6XA-T076. The PMIP3, PMIP4 and LOVECLIM multi-model mean data can be found at http://hdl.handle.net/1959.4/100036. PMIP3 data can be found at https://esgf-node.llnl.gov/search/cmip5/ and most PMIP4 data can be found at https://esgf-data.dkrz.de/search/cmip6-dkrz/.

Author contributions. RAG performed the data analysis. LM and KJM conceived the study and provided support to the interpretation of results. XC compiled existing sea-ice proxy data and provided expert knowledge on sea-ice processes and sea-ice proxy data. RAG wrote the manuscript with contributions from LM, KJM and XC. DC, GL, WRP, XS and JZ provided the PMIP4 model outputs presented in this paper. All authors contributed to the final version of the manuscript.

Competing interests. The authors declare that they have no conflict of interest.

Acknowledgements. This research is a result of the Past Global Changes (PAGES) working group 'Cycles of Sea-Ice Dynamics in the Earth system' (C-SIDE). We thank Masa Kageyama for providing the PMIP4 LGM outputs of the IPSL model. Ryan Green was supported by a summer scholarship provided by the Australian Research Council Centre of Excellence for Climate Extremes (CE170100023), and UNSW (through Laurie Menviel's UNSW Scientia fellowship). Laurie Menviel and Katrin Meissner are thankful for funding from the Australian Research Council (FT180100606, DP18010004, DP180102357). Computational resources were provided by the NCI National Facility at the Australian National University, through awards under the National Computational Merit Allocation Scheme, the Intersect allocation scheme, and the UNSW HPC at NCI Scheme.

References

Abe-Ouchi, A., Saito, F., Kawamura, K., Raymo, M., Okuno, J., Takahashi, K., and Blatter, H.: Insolation-driven 100,000-year glacial cycles and hysteresis of ice-sheet volume, Nature, 500, 190–193, 2013.

Abe-Ouchi, A., Saito, F., Kageyama, M., Braconnot, P., Harrison, S. P., Lambeck, K., Otto-Bliesner, B. L., Peltier, W. R., Tarasov, L., Peterschmitt, J.-Y., and Takahashi, K.: Ice-sheet configuration in the CMIP5/PMIP3 Last Glacial Maximum experiments, Geoscientific Model Development, 8, 3621–3637, https://doi.org/10.5194/gmd-8-3621-2015, https://www.geosci-model-dev.net/8/3621/2015/, 2015.

Abelmann, A., Gersonde, R., Knorr, G., Zhang, X., Chapligin, B., Maier, E., Esper, O., Friedrichsen, H., Lohmann, G., Meyer, H., et al.: The seasonal sea-ice zone in the glacial Southern Ocean as a carbon sink, Nature communications, 6, 1–13, 2015.

Adkins, J., McIntyre, K., and Schrag, D.: The salinity, temperature, and δ^{18}O of the glacial deep ocean, Science, 298, 1769–1773, 2002.

Allen, C., Pike, J., and Pudsey, C.: Last glacial-interglacial sea-ice cover in the SW Atlantic and its potential role in global deglaciation, Quaternary Science Reviews, 30, 2446–2458, 2011.

Argus, D. F., Peltier, W., Drummond, R., and Moore, A. W.: The Antarctica component of postglacial rebound model ICE-6G_C (VM5a) based on GPS positioning, exposure age dating of ice thicknesses, and relative sea level histories, Geophysical Journal International, 198, 537–563, 2014.

Bentley, M. J., Cofaigh, C., Anderson, J. B., Conway, H., Davies, B., Graham, A. G., Hillenbrand, C.-D., Hodgson, D. A., Jamieson, S. S., Larter, R. D., Mackintosh, A., Smith, J. A., Verleyen, E., Ackert, R. P., Bart, P. J., Berg, S., Brunstein, D., Canals, M., Colhoun, E. A., Crosta, X., Dickens, W. A., Domack, E., Dowdeswell, J. A., Dunbar, R., Ehrmann, W., Evans, J., Favier, V., Fink, D., Fogwill, C. J., Glasser, N. F., Gohl, K., Golledge, N. R., Goodwin, I., Gore, D. B., Greenwood, S. L., Hall, B. L., Hall, K., Hedding, D. W., Hein, A. S., Hocking, E. P., Jakobsson, M., Johnson, J. S., Jomelli, V., Jones, R. S., Klages, J. P., Kristoffersen, Y., Kuhn, G., Leventer, A., Licht, K., Lilly, K., Lindow, J., Livingstone, S. J., Massé, G., McGlone, M. S., McKay, R. M., Melles, M., Miura, H., Mulvaney, R., Nel, W., Nitsche, F. O., O'Brien, P. E., Post, A. L., Roberts, S. J., Saunders, K. M., Selkirk, P. M., Simms, A. R., Spiegel, C., Stolldorf, T. D., Sugden, D. E., van der Putten, N., van Ommen, T., Verfaillie, D., Vyverman, W., Wagner, B., White, D. A., Witus, A. E., and Zwartz, D.: A community-based geological reconstruction of Antarctic Ice Sheet deglaciation since the Last Glacial Maximum, Quaternary Science Reviews, 100, 1 – 9, https://doi.org/https://doi.org/10.1016/j.quascirev.2014.06.025, http://www.sciencedirect.com/science/article/pii/S0277379114002546, reconstruction of Antarctic Ice Sheet Deglaciation (RAISED), 2014.

Benz, V., Esper, O., Gersonde, R., Lamy, F., and Tiedemann, R.: Last Glacial Maximum sea surface temperature and sea-ice extent in the Pacific sector of the Southern Ocean, Quaternary Science Reviews, 146, 216–237, 2016.

Bouttes, N., Roche, D., and Paillard, D.: Systematic study of the impact of fresh water fluxes on the glacial carbon cycle, Climate of the Past, 8, 589–607, 2012.

Bracegirdle, T. J., Stephenson, D. B., Turner, J., and Phillips, T.: The importance of sea ice area biases in 21st century multimodel projections of Antarctic temperature and precipitation, Geophysical Research Letters, 42, 10–832, 2015.

Braconnot, P. and Kageyama, M.: Shortwave forcing and feedbacks in Last Glacial Maximum and Mid-Holocene PMIP3 simulations, Philosophical Transactions of the Royal Society A: Mathematical, Physical and Engineering Sciences, 373, 20140 424, 2015.

Brady, E. C., Otto-Bliesner, B. L., Kay, J. E., and Rosenbloom, N.: Sensitivity to glacial forcing in the CCSM4, Journal of Climate, 26, 1901–1925, 2013.

Carlson, A. and Winsor, K.: Northern Hemisphere ice-sheet responses to past climate warming, Nature Geoscience, 5, 507 –613, https://doi.org/10.1038/ngeo1528, 2012.

Cavalieri, D. J. and Parkinson, C. L.: Arctic sea ice variability and trends, 1979-2010, The Cryosphere, 6, 881, 2012.

Chandan, D. and Peltier, W. R.: Regional and global climate for the mid-Pliocene using the University of Toronto version of CCSM4 and PlioMIP2 boundary conditions, Climate of the Past, 13, 919–942, 2017.

Chandan, D. and Peltier, W. R.: On the mechanisms of warming the mid-Pliocene and the inference of a hierarchy of climate sensitivities with relevance to the understanding of climate futures, Climate of the Past, 14, 825–856, 2018.

Clark, P. U., Dyke, A. S., Shakun, J. D., Carlson, A. E., Clark, J., Wohlfarth, B., Mitrovica, J. X., Hostetler, S. W., and McCabe, A. M.: The last glacial maximum, science, 325, 710–714, 2009.

CLIMAP-Project-Members: Map and Chart Ser. MC-36, chap. Seasonal reconstruction of the Earth surface at the last glacial maximum, Lamont-Doherty Geological Observatory of Columbia University, Palisades, 1981.

Crosta, X., Pichon, J., and Burckle, L.: Application of modern analog technique to marine Antarctic diatoms: Reconstruction of maximum sea-ice extent at the Last Glacial Maximum, Paleoceanography, 13, 284–297, 1998.

Doddridge, E. W. and Marshall, J.: Modulation of the seasonal cycle of Antarctic sea ice extent related to the Southern Annular Mode, Geophysical Research Letters, 44, 9761–9768, 2017.

Dufresne, J.-L., Foujols, M.-A., Denvil, S., Caubel, A., Marti, O., Aumont, O., Balkanski, Y., Bekki, S., Bellenger, H., Benshila, R., et al.: Climate change projections using the IPSL-CM5 Earth System Model: from CMIP3 to CMIP5, Climate dynamics, 40, 2123–2165, 2013.

Eayrs, C., Holland, D., Francis, D., Wagner, T., Kumar, R., and Li, X.: Understanding the Seasonal Cycle of Antarctic Sea Ice Extent in the Context of Longer-Term Variability, Reviews of Geophysics, 57, 1037–1064, 2019.

Eayrs, C., Li, X., Raphael, M. N., and Holland, D. M.: Rapid decline in Antarctic sea ice in recent years hints at future change, Nature Geoscience, 14, 460–464, 2021.

Elderfield, H., Greaves, M., Barker, S., Hall, I. R., Tripati, A., Ferretti, P., Crowhurst, S., Booth, L., and Daunt, C.: A record of bottom water temperature and seawater δ18O for the Southern Ocean over the past 440 kyr based on Mg/Ca of benthic foraminiferal Uvigerina spp., Quaternary Science Reviews, 29, 160–169, 2010.

Esper, O. and Gersonde, R.: Quaternary surface water temperature estimations: New diatom transfer functions for the Southern Ocean, Palaeogeography, Palaeoclimatology, Palaeoecology, 414, 1–19, 2014a.

Esper, O., Gersonde, R., and Lohmann, G.: Southern Ocean surface temperature and sea ice fields during the Last Interglacial, AGUFM, 2014b, PP21G–06, 2014b.

Ferrari, R., Jansen, M. F., Adkins, J. F., Burke, A., Stewart, A. L., and Thompson, A. F.: Antarctic sea ice control on ocean circulation in present and glacial climates, Proceedings of the National Academy of Sciences, 111, 8753–8758, 2014.

Ferreira, D., Marshall, J., Bitz, C. M., Solomon, S., and Plumb, A.: Antarctic Ocean and sea ice response to ozone depletion: A two-time-scale problem, Journal of Climate, 28, 1206–1226, 2015.

Ferry, A. J., Crosta, X., Quilty, P. G., Fink, D., Howard, W., and Armand, L. K.: First records of winter sea ice concentration in the southwest Pacific sector of the Southern Ocean, Paleoceanography, 30, 1525–1539, 2015.

Frölicher, T. L., Sarmiento, J. L., Paynter, D. J., Dunne, J. P., Krasting, J. P., and Winton, M.: Dominance of the Southern Ocean in anthropogenic carbon and heat uptake in CMIP5 models, Journal of Climate, 28, 862–886, 2015.

Galbraith, E. and de Lavergne, C.: Response of a comprehensive climate model to a broad range of external forcings: relevance for deep ocean ventilation and the development of late Cenozoic ice ages, Climate Dynamics, 52, 653–679, 2019.

Gent, P. R., Danabasoglu, G., Donner, L. J., Holland, M. M., Hunke, E. C., Jayne, S. R., Lawrence, D. M., Neale, R. B., Rasch, P. J., Vertenstein, M., et al.: The community climate system model version 4, Journal of climate, 24, 4973–4991, 2011.

Gersonde, R., Crosta, X., Abelmann, A., and Armand, L.: Sea-surface temperature and sea ice distribution of the Southern Ocean at the EPILOG Last Glacial Maximum - A circum-Antarctic view based on siliceous microfossil records, Quaternary Science Reviews, 24, 869–896, 2005.

Ghadi, P., Nair, A., Crosta, X., Mohan, R., Manoj, M., and Meloth, T.: Antarctic sea-ice and palaeoproductivity variation over the last 156,000 years in the Indian sector of Southern Ocean, Marine Micropaleontology, 160, 101 894, 2020.

Giorgetta, M. A., Jungclaus, J., Reick, C. H., Legutke, S., Bader, J., Böttinger, M., Brovkin, V., Crueger, T., Esch, M., Fieg, K., et al.: Climate and carbon cycle changes from 1850 to 2100 in MPI-ESM simulations for the Coupled Model Intercomparison Project phase 5, Journal of Advances in Modeling Earth Systems, 5, 572–597, 2013.

Goosse, H., Brovkin, V., Fichefet, T., Jongma, J., Huybrechts, P., Mouchet, A., Barriat, P.-Y., Campin, J.-M., Deleersnijder, E., Driesschaert, E., Goelzer, H., Haarsma, R., Janssens, Y., Loutre, M.-F., Maqueda, M. A. M., Opsteegh, T., Mathieu, P.-P., Munhoven, G., Petterson, E., Renssen, H., Roche, D., Schaeffer, M., Selten, F., Severijns, C., Tartinville, B., and Weber, N.: Description of the Earth system model of intermediate complexity LOVECLIM version 1.2., Geoscientific Model Development, 3, 603–633, 2010.

Goosse, H., Roche, D., Mairesse, A., and Berger, M.: Modelling past sea ice changes, Quaternary Science Reviews, 79, 191–206, 2013.

Hajima, T., Watanabe, M., Yamamoto, A., Tatebe, H., Noguchi, M. A., Abe, M., Ohgaito, R., Ito, A., Yamazaki, D., Okajima, H., et al.: Development of the MIROC-ES2L Earth system model and the evaluation of biogeochemical processes and feedbacks, Geoscientific Model Development, 13, 2197–2244, 2020.

Haumann, F. A., Gruber, N., Münnich, M., Frenger, I., and Kern, S.: Sea-ice transport driving Southern Ocean salinity and its recent trends, Nature, 537, 89–92, 2016.

Holland, P. R. and Kwok, R.: Wind-driven trends in Antarctic sea-ice drift, Nature Geoscience, 5, 872–875, 2012.

Howe, J., Piotrowski, A., Noble, T., Mulitza, S., Chiessi, C., and Bayon, G.: North Atlantic Deep Water Production during the Last Glacial Maximum, Nature Communications, 7, doi:10.1038/ncomms11 765, 2016.

Ivanovic, R., Gregoire, L., Kageyama, M., Roche, D., Valdes, P., Burke, A., Drummond, R., Peltier, W., and Tarasov, L.: Transient climate simulations of the deglaciation 21-9 thousand years before present (version 1) - PMIP4 Core experiment design and boundary conditions, Geoscientific Model Development, 9, 2563 – 2587, 2016.

Jaccard, S. L., Hayes, C. T., Martinez-Garcia, A., Hodell, D. A., Anderson, R. F., Sigman, D. M., and Haug, G.: Two modes of change in Southern Ocean productivity over the past million years, Science, 339, 1419–1423, 2013.

Kageyama, M., Braconnot, P., Bopp, L., Caubel, A., Foujols, M.-A., Guilyardi, E., Khodri, M., Lloyd, J., Lombard, F., Mariotti, V., et al.: Mid-Holocene and Last Glacial Maximum climate simulations with the IPSL model—Part I: Comparing IPSL_CM5A to IPSL_CM4, Climate dynamics, 40, 2447–2468, 2013.

Kageyama, M., Albani, S., Braconnot, P., Harrison, S. P., Hopcroft, P. O., Ivanovic, R. F., Lambert, F., Marti, O., Pe ltier, W. R., Peterschmitt, J.-Y., Roche, D. M., Tarasov, L., Zhang, X., Brady, E. C., Haywood, A. M., LeGrande, A. N., Lunt, D. J., Mahowald, N. M., Mikolajewicz, U., Nisancioglu, K. H., Otto-Bliesner, B. L., Renssen, H., Tomas, R. A., Zhang, Q., Abe-Ouch i, A., Bartlein, P. J., Cao, J., Li, Q., Lohmann, G., Ohgaito, R., Shi, X., Volodin, E., Yoshida, K., Zhang, X., and Zheng, W.: The PMIP4 contribution to CMIP6 – Part 4: Scientific objectives and experimental design of the PMIP4-CMIP6 Last Glacial Maximum experiments and PMIP4 sensitivity experiments, Geoscientific Model Development, 10, 4035–4055, https://doi.org/10.5194/gmd-10-4035-2017, https://www.geosci-model-dev.net/10/4035/2017/, 2017.

Kageyama, M., Harrison, S. P., Kapsch, M.-L., Löfverström, M., Lora, J. M., Mikolajewicz, U., Sherriff-Tadano, S., Vadsaria, T., Abe-Ouchi, A., Bouttes, N., Chandan, D., LeGrande, A. N., Lhardy, F., Lohmann, G., Morozova, P. A., Ohgaito, R., Peltier, W. R., Quiquet, A., Roche,

D. M., Shi, X., Schmittner, A., Tierney, J. E., and Volodin, E.: The PMIP4-CMIP6 Last Glacial Maximum experiments: preliminary results and comparison with the PMIP3-CMIP5 simulations, Climate of the Past Discussions, 2020, 1–37, https://doi.org/10.5194/cp-2019-169, https://www.clim-past-discuss.net/cp-2019-169/, 2020.

Kageyama, M., Harrison, S. P., Kapsch, M.-L., Lofverstrom, M., Lora, J. M., Mikolajewicz, U., Sherriff-Tadano, S., Vadsaria, T., Abe-Ouchi, A., Bouttes, N., et al.: The PMIP4 Last Glacial Maximum experiments: preliminary results and comparison with the PMIP3 simulations, Climate of the Past, 17, 1065–1089, 2021.

Kidston, M., Matear, R., and Baird, M.: Parameter optimisation of a marine ecosystem model at two contrasting stations in the Sub-Antarctic Zone, Deep-Sea Research II, 58, 2301–2315, 2011.

Klockmann, M., Mikolajewicz, U., and Marotzke, J.: The effect of greenhouse gas concentrations and ice sheets on the glacial AMOC in a coupled climate model, Climate of the Past, 12, 1829–1846, 2016.

Kohfeld, K., Graham, R., de Boer, A., Sime, L., Wolff, E., Qur, C. L., and Bopp, L.: Southern Hemisphere westerly wind changes during the Last Glacial Maximum: paleo-data synthesis, Quaternary Science Reviews, 68, 76–95, https://doi.org/https://doi.org/10.1016/j.quascirev.2013.01.017, 2013.

Kohfeld, K. E. and Chase, Z.: Temporal evolution of mechanisms controlling ocean carbon uptake during the last glacial cycle, Earth and Planetary Science Letters, 472, 206–215, 2017.

Landschützer, P., Gruber, N., Haumann, F. A., Rödenbeck, C., Bakker, D. C. E., van Heuven, S., Hoppema, M., Metzl, N., Sweeney, C., Takahashi, T., Tilbrook, B., and Wanninkhof, R.: The reinvigoration of the Southern Ocean carbon sink, Science, 349, 1221–1224, https://doi.org/10.1126/science.aab2620, http://science.sciencemag.org/content/349/6253/1221, 2015.

Lhardy, F., Bouttes, N., Roche, D. M., Crosta, X., Waelbroeck, C., and Paillard, D.: Impact of Southern Ocean surface conditions on deep ocean circulation during the LGM: a model analysis, Climate of the Past, 17, 1139–1159, 2021.

Li, L., Lin, P., Yu, Y., Wang, B., Zhou, T., Liu, L., Liu, J., Bao, Q., Xu, S., Huang, W., et al.: The flexible global ocean-atmosphere-land system model, grid-point version 2: FGOALS-g2, Advances in Atmospheric Sciences, 30, 543–560, 2013.

Locarnini, R., Mishonov, A., Antonov, J., Boyer, T., Garcia, H., Baranova, O., Zweng, M., and Johnson, D.: NOAA Atlas NESDIS 68 WORLD OCEAN ATLAS 2009, vol. 1: Temperature, Tech. rep., technical report march, US Gov. Print. Off., Washington, DC, 2010.

Lynch-Stieglitz, J., Adkins, J. F., Curry, W. B., Dokken, T., Hall, I. R., Herguera, J. C., Hirschi, J. J.-M., Ivanova, E. V., Kissel, C., Marchal, O., et al.: Atlantic meridional overturning circulation during the Last Glacial Maximum, science, 316, 66–69, 2007.

Marcott, S., Bauska, T., Buizert, C., Steig, E., Rosen, J., Cuffey, K., Fudge, T., Severinghaus, J., Ahn, J., Kalk, M., McConnell, J., Sowers, T., Taylor, K., White, J., and Brook, E.: Centennial-scale changes in the global carbon cycle during the last deglaciation, Nature, 514, 616–619, https://doi.org/10.1038/nature13799, 2014.

Marzocchi, A. and Jansen, M. F.: Connecting Antarctic sea ice to deep?ocean circulation in modern and glacial climate simulations, Geophysical Research Letters, 44, 6286–6295, https://doi.org/10.1002/2017GL073936, 2017.

Massom, R., Scambos, T., Bennetts, L., Reid, P., Squire, V., and Stammerjohn, S.: Antarctic ice shelf disintegration triggered by sea ice loss and ocean swell, Nature, 558, 383–389, https://doi.org/10.1038/s41586-018-0212-1, 2018.

Mauritsen, T., Bader, J., Becker, T., Behrens, J., Bittner, M., Brokopf, R., Brovkin, V., Claussen, M., Crueger, T., Esch, M., et al.: Developments in the MPI-M Earth System Model version 1.2 (MPI-ESM1. 2) and its response to increasing CO2, Journal of Advances in Modeling Earth Systems, 11, 998–1038, 2019.

Mayewski, P., Carleton, A., Birkel, S., Dixon, D., Kurbatov, A., Korotkikh, E., McConnell, J., Curran, M., Cole-Dai, J., Jiang, S., et al.: Ice core and climate reanalysis analogs to predict Antarctic and Southern Hemisphere climate changes, Quaternary Science Reviews, 155, 50–66, 2017.

Meijers, A.: The Southern Ocean in the coupled model intercomparison project phase 5, Philosophical Transactions of the Royal Society A: Mathematical, Physical and Engineering Sciences, 372, 20130 296, 2014.

Meissner, K., Schmittner, A., Weaver, A., and Adkins, J.: The ventilation of the North Atlantic Ocean during the Last Glacial Maximum - a comparison between simulated and observed radiocarbon ages, Paleoceanography, 18, DOI:10.1029/2002PA000 762, 2003.

Menviel, L., Timmermann, A., Mouchet, A., and Timm, O.: Climate and marine carbon cycle response to changes in the strength of the southern hemispheric westerlies, Paleoceanography, 23, doi:10.1029/2007PA001 604, 2008.

Menviel, L., Yu, J., Joos, F., Mouchet, A., Meissner, K., and England, M.: Poorly ventilated deep ocean at the Last Glacial Maximum inferred from carbon isotopes: a data-model comparison study, Paleoceanography, 32, 2–17, https://doi.org/10.1002/2016PA003024, 2017.

Menviel, L. C., Spence, P., Skinner, L. C., Tachikawa, K., Friedrich, T., Missiaen, L., and Yu, J.: Enhanced Mid-depth Southward Transport in the Northeast Atlantic at the Last Glacial Maximum Despite a Weaker AMOC, Paleoceanography and Paleoclimatology, 35, e2019PA003 793, https://doi.org/10.1029/2019PA003793, https://agupubs.onlinelibrary.wiley.com/doi/abs/10.1029/2019PA003793, e2019PA003793 10.1029/2019PA003793, 2020.

Mikaloff-Fletcher, S., Gruber, N., Jacobson, A., Doney, S., Dutkiewicz, S., Gerber, M., Follows, M., Joos, F., Lindsay, K., Menemenlis, D., Mouchet, A., Müller, S., and Sarmiento, J.: Inverse estimates of anthropogenic CO_2 uptake, tranport, and storage by the ocean, Global Biogeochemical Cycles, 20, GB2002, https://doi.org/10.1029/2005GB002530, 2006.

Muglia, J. and Schmittner, A.: Glacial Atlantic overturning increased by wind stress in climate models, Geophysical Research Letters, 42, 9862–9868, https://doi.org/10.1002/2015GL064583, https://agupubs.onlinelibrary.wiley.com/doi/abs/10.1002/2015GL064583, 2015.

Nair, A., Mohan, R., Crosta, X., Manoj, M., Thamban, M., and Marieu, V.: Southern Ocean sea ice and frontal changes during the Late Quaternary and their linkages to Asian summer monsoon, Quaternary Science Reviews, 213, 93–104, 2019.

Oka, A., Hasumi, H., and Abe-Ouchi, A.: The thermal threshold of the Atlantic meridional overturning circulation and its control by wind stress forcing during glacial climate, Geophysical Research Letters, 39, https://doi.org/10.1029/2012GL051421, https://agupubs.onlinelibrary.wiley.com/doi/abs/10.1029/2012GL051421, 2012.

Parkinson, C. L.: A 40-y record reveals gradual Antarctic sea ice increases followed by decreases at rates far exceeding the rates seen in the Arctic, Proceedings of the National Academy of Sciences, 116, 14 414–14 423, https://doi.org/10.1073/pnas.1906556116, https://www.pnas.org/content/116/29/14414, 2019.

Peltier, W., Argus, D., and Drummond, R.: Space geodesy constrains ice-age terminal deglaciation: The global ICE-6G-C (VM5a) model, J. Geophys. Res. Solid Earth, 120, 450–487, https://doi.org/doi:10.1002/2014JB011176, 2015.

Peltier, W. R. and Vettoretti, G.: Dansgaard-Oeschger oscillations predicted in a comprehensive model of glacial climate: A "kicked" salt oscillator in the Atlantic, Geophysical Research Letters, 41, 7306–7313, https://doi.org/10.1002/2014GL061413, https://agupubs.onlinelibrary.wiley.com/doi/abs/10.1002/2014GL061413, 2014.

Purich, A., Cai, W., England, M., and Cowan, T.: Evidence for link between modelled trends in Antarctic sea ice and underestimated westerly wind changes, Nature Communications, 7, 10 409, https://doi.org/10.1038/ncomms10409, 2016.

Roche, D., Crosta, X., and Renssen, H.: Evaluating Southern Ocean sea-ice for the Last Glacial Maximum and pre-industrial climates: PMIP-2 models and data evidence, Quaternary Science Reviews, 56, 99–106, 2012.

Sabine, C., Feely, R., Gruber, N., Key, R., Lee, K., Bullister, J., Wanninkhof, R., Wong, C., Wallace, D., Tilbrook, B., Millero, F., Peng, T.-H., Kozyr, A., Ono, T., and Rios, A.: The oceanic sink of anthropogenic CO_2, Science, 305, 367–371, 2004.

Scambos, T. A., Bohlander, J., Shuman, C. A., and Skvarca, P.: Glacier acceleration and thinning after ice shelf collapse in the Larsen B embayment, Antarctica, Geophysical Research Letters, 31, 2004.

Schmidt, G. A., Jungclaus, J. H., Ammann, C. M., Bard, E., Braconnot, P., Crowley, T. J., Delaygue, G., Joos, F., Krivova, N. A., Muscheler, R., Otto-Bliesner, B. L., Pongratz, J., Shindell, D. T., Solanki, S. K., Steinhilber, F., and Vieira, L. E. A.: Climate forcing reconstructions for use in PMIP simulations of the last millennium (v1.0), Geosci. Model Dev., 4, 33–45, https://doi.org/10.5194/gmd-4-33-2011, 2011.

Schmidt, G. A., Kelley, M., Nazarenko, L., Ruedy, R., Russell, G. L., Aleinov, I., Bauer, M., Bauer, S. E., Bhat, M. K., Bleck, R., et al.: Configuration and assessment of the GISS ModelE2 contributions to the CMIP5 archive, Journal of Advances in Modeling Earth Systems, 6, 141–184, 2014.

Schulzweida, U., Kornblueh, L., and Quast, R.: CDO: Climate Data Operators v1. 6.4, Cent. Mar. Atmos. Sci..(ZMAW). Max-Planck Inst. Meteorol. Univ. Hamburg. https://code. zmaw. de/projects/cdo (last access August 2014), 2014.

Schweitzer, P. N.: Monthly average polar sea-ice concentration: US Geological Survey digital data series DDS-27, US Geological Survey, Reston, Virginia. Dataset information available online at http://pubs. usgs. gov/dds/dds27, 1995.

Sepulchre, P., Caubel, A., Ladant, J.-B., Bopp, L., Boucher, O., Braconnot, P., Brockmann, P., Cozic, A., Donnadieu, Y., Dufresne, J.-L., et al.: IPSL-CM5A2–an Earth system model designed for multi-millennial climate simulations, Geoscientific Model Development, 13, 3011–3053, 2020.

Sidorenko, D., Rackow, T., Jung, T., Semmler, T., Barbi, D., Danilov, S., Dethloff, K., Dorn, W., Fieg, K., Gößling, H. F., et al.: Towards multi-resolution global climate modeling with ECHAM6–FESOM. Part I: model formulation and mean climate, Climate Dynamics, 44, 757–780, 2015.

Sigman, D. and Boyle, E.: Glacial/interglacial variations in atmospheric carbon dioxide, Nature, 407, 859–869, 2000.

Sime, L. C., Hodgson, D., Bracegirdle, T. J., Allen, C., Perren, B., Roberts, S., and de Boer, A. M.: Sea ice led to poleward-shifted winds at the Last Glacial Maximum: the influence of state dependency on CMIP5 and PMIP3 models, Climate of the Past, 12, 2241–2253, https://doi.org/10.5194/cp-12-2241-2016, https://www.clim-past.net/12/2241/2016/, 2016.

Skinner, L., Primeau, F., Freeman, E., de la Fuente, M., Goodwin, P., Gottschalk, J., Huang, E., McCave, I., Noble, T., and Scrivner, A.: Radiocarbon constraints on the glacial ocean circulation and its impact on atmospheric CO_2, Nature Communications, 8, 16 010, https://doi.org/10.1038/ncomms16010, 2017.

Sueyoshi, T., Ohgaito, R., Yamamoto, A., Chikamoto, M., Hajima, T., Okajima, H., Yoshimori, M., Abe, M., O'ishi, R., Saito, F., et al.: Set-up of the PMIP3 paleoclimate experiments conducted using an Earth system model, MIROC-ESM, Geoscientific Model Development, 6, 819–836, 2013.

Tierney, J. E., Zhu, J., King, J., Malevich, S. B., Hakim, G. J., and Poulsen, C. J.: Glacial cooling and climate sensitivity revisited, Nature, 584, 569–573, 2020.

Ullman, D., Legrande, A., Carlson, A., Anslow, F., and Licciardi, J.: Assessing the impact of Laurentide Ice Sheet topography on glacial climate, Climate of the Past, 10, 487–507, 2014.

Voldoire, A., Sanchez-Gomez, E., y Mélia, D. S., Decharme, B., Cassou, C., Sénési, S., Valcke, S., Beau, I., Alias, A., Chevallier, M., et al.: The CNRM-CM5. 1 global climate model: description and basic evaluation, Climate dynamics, 40, 2091–2121, 2013.

Waelbroeck, C., Paul, A., Kucera, M., Rosell-Melé, A., Weinelt, M., Schneider, R., Mix, A., Abelmann, A., Armand, L., Bard, E., Barker, S., Barrows, T., Benway, H., Cacho, I., Chen, M., Cortijo, E., Crosta, X., de Vernal, A., Dokken, T., Duprat, J., Elderfield, H., Eynaud, F.,

Gersonde, G., Hayes, A., Henry, M., Hillaire-Marcel, C., Huang, C., Jansen, E., Juggins, S., Kallel, N., Kiefer, T., Kienast, M., Labeyrie, L., Leclaire, H., Londeix, L., Mangin, S., Matthiessen, J., Marret, F., Meland, M., Morey, A., Mulitza, S., Pflaumann, U., Pisias, N., Radi, T., Rochon, A., Rohling, E., Sbaffi, L., Schaefer-Neth, C., Solignac, S., Spero, H., Tachikawa, K., Turon, J., and project members, M.: Constraints on the magnitude and patterns of ocean cooling at the Last Glacial Maximum, Nature Geoscience, 2, 127–132, 2009.

Wang, G., Hendon, H. H., Arblaster, J. M., Lim, E.-P., Abhik, S., and van Rensch, P.: Compounding tropical and stratospheric forcing of the record low Antarctic sea-ice in 2016, Nature communications, 10, 1–9, 2019.

Watanabe, M., Chikira, M., Imada, Y., and Kimoto, M.: Convective control of ENSO simulated in MIROC, Journal of Climate, 24, 543–562, 2011.

Watson, A. J., Schuster, U., Shutler, J. D., Holding, T., Ashton, I. G., Landschützer, P., Woolf, D. K., and Goddijn-Murphy, L.: Revised estimates of ocean-atmosphere CO 2 flux are consistent with ocean carbon inventory, Nature communications, 11, 1–6, 2020.

Xiao, W., Esper, O., and Gersonde, R.: Last Glacial-Holocene climate variability in the Atlantic sector of the Southern Ocean, Quaternary Science Reviews, 135, 115–137, 2016.

Yukimoto, S., Adachi, Y., Hosaka, M., Sakami, T., Yoshimura, H., Hirabara, M., Tanaka, T. Y., Shindo, E., Tsujino, H., Deushi, M., et al.: A new global climate model of the Meteorological Research Institute: MRI-CGCM3—Model description and basic performance—, Journal of the Meteorological Society of Japan. Ser. II, 90, 23–64, 2012.

Zheng, F., Li, J., Clark, R., and Nnamchi, H.: Simulation and Projection of the Southern Hemisphere Annular Mode in CMIP5 Models, Journal of Climate, 26, 9860–9879, https://doi.org/10.1175/JCLI-D-13-00204.1, 2013.

Zheng, W. and Yu, Y.: Paleoclimate simulations of the mid-Holocene and Last Glacial Maximum by FGOALS, Advances in Atmospheric Sciences, 30, 684–698, 2013.